

Searching for saturation in forward dijet production at the LHC

A. van Hameren ^a, H. Kakkad ^b, P. Kotko ^b,
K. Kutak ^a, S. Sapeta ^a

^a *Institute of Nuclear Physics, Polish Academy of Sciences
Radzikowskiego 152, 31-342 Kraków, Poland*

^b *AGH University Of Krakow,
Faculty of Physics and Applied Computer Science,
al. Mickiewicza 30, 30-059 Kraków, Poland*

Abstract

We review recent results for forward jets at the LHC and EIC as obtained within small- x Improved Transverse Momentum Dependent factorization (ITMD). In addition to elementary overview of various approaches to perturbative QCD at high energy, including High Energy Factorization, Color Glass Condensate and ITMD, we describe the Monte Carlo implementation and discuss the existing and unpublished phenomenological results for forward dijets.

1 Introduction

Quantum Chromodynamics (QCD) is a well established theory that describes interactions of quarks and gluons. However, it still has its challenges. In the high energy domain, one of the long standing problems is finding clear experimental signals of gluon saturation, which is a signature of quasi equilibrium between gluon splitting and gluon fusion in dense nuclear systems. Gluon saturation has been predicted from QCD long time ago [1, 2] and has been extensively studied using various approaches, most recently the Color Glass Condensate (CGC) – *i.e.* effective theory obtained within QCD (for a reviews see [3–7] and the textbook [8]).

While there is no doubt that gluon distributions must saturate at some point due to the unitarity constraints on the cross section, and there are strong indications of saturation in the data [9–20], a complete consensus on reaching it is still to be achieved. This is mainly due to the demanding kinematics. It requires the final states to be measured in the forward region of the detectors and dealing with nuclear targets, which poses additional challenges due to the rich collision environment (see *e.g.* [21]). Moreover, theoretical predictions in high energy QCD are at present not as precise as those requiring ordinary collinear factorization.

Among various final states that can be measured in the context of saturation searches, the system consisting of two identified jets in the forward region (and everything else) plays a special role [22–24]. In addition to the possibility of studying correlations, it has an important advantage over the single-inclusive jet production. Namely, the jet transverse momenta can be quite large, of the order of twenty GeV or so, and still be sensitive to the saturation effects in the back-to-back region. In single inclusive jet production, the jet transverse momentum is demanded to be of the order of the saturation scale Q_s and determines the average transverse momenta of gluons being “saturated”. The latter is of the order of a few GeV, for sufficiently high collision energy and sufficiently forward. Jets with larger transverse momenta are easier to reconstruct and are “cleaner”. Moreover, on theoretical grounds, the description of harder dijets becomes possible

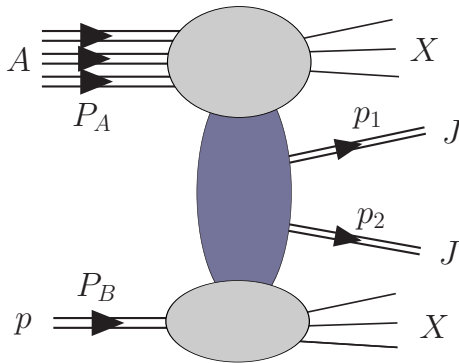


Figure 1: The momentum assignment in the inclusive dijet production in p+A collision. The multiple double lines represent the nuclear target A . J are the jets with momenta p_1 and p_2 . X denotes arbitrary final states.

in terms of “generalized” transverse momentum dependent (TMD) factorization, which makes it easier to implement in Monte Carlo generators than the full CGC.

Dijet yields at relatively forward rapidity have already been measured at the Large Hadron Collider (LHC) by ATLAS collaboration for both proton-proton and proton-lead collisions [25]. Since there was no cross sections measurement, the conclusions regarding saturation signals do not give yet a definite answer to whether saturation has been observed or not. Inclusive single forward jet energy spectra for proton-lead collisions measured at CMS CASTOR detector [26] does not provide convincing proof either. Further research and analysis are necessary to gain a better understanding of gluon saturation and its effects on nuclear systems. In particular, more measurements of both proton-proton and proton-lead collisions in the same kinematics are needed. In addition to the ATLAS forward detector, the ALICE collaboration plans to build a more forward detector FoCal [27] that hopefully will shed more light on the saturation phenomenon. The forward jet physics at LHC is complementary to the physics of the Electron Ion Collider (EIC) [28, 29] one of the primarily goals of which is to study gluon saturation physics.

In this work, we review the theoretical framework suitable for a description of forward dijet production in hadro and lepto-production in the full azimuthal angle range. The formalism lies in the intersection of the CGC theory and more traditional factorization approach, utilizing TMD gluon distributions. Since the formalism accounts for power corrections it has been dubbed as Improved TMD Factorization (ITMD) [30]. A review of some essential aspects of high energy QCD and the ITMD framework itself is contained in Section 2. We shall also review Monte Carlo implementation of the ITMD framework KATIE (Section 3), construction of the TMD gluon distributions, as well as recent phenomenological predictions for azimuthal dijet correlations, both for proton-proton and proton-lead collisions, in the kinematics of the forward calorimeters of ATLAS detector and planned FoCal of ALICE (Section 4). We also include new unpublished earlier computations of the rapidity distributions for different kinematic cuts.

2 Forward dijet production in high energy QCD

2.1 Kinematics

The process in question is the inclusive production of two jet, that is, there are at least two jets with transverse momenta above a certain threshold, and both are produced in the forward rapidity interval in the center of mass frame:

$$A(P_A) + p(P_B) \rightarrow J(p_1) + J(p_2) + X, \quad (1)$$

where A is either the proton state p or a nucleus having the four momentum P_A that is hit by the proton state with four momentum P_B (see Fig. 1). The produced jets have four momenta p_1 and p_2 and are defined by a proper jet algorithm. X corresponds to other particles produced in the

process; there are no kinematic cuts imposed on those additional states. We shall also discuss the complementary DIS process

$$A(P_A) + e^-(P_B) \rightarrow J(p_1) + J(p_2) + e^-(P'_B) + X, \quad (2)$$

which will be studied at EIC and will be essential in testing the theoretical formalism and constraining the nonperturbative input.

In what follows, we define the P_A and P_B four momenta as being the two light cone vectors, defining the “plus” and “minus” light cone components:

$$P_A^\mu = (E_A, 0, 0, -E_A) = E_A n_+^\mu, \quad P_B^\mu = (E_B, 0, 0, E_B) = E_B n_-^\mu, \quad (3)$$

with the center of mass energy $s = 2P_A \cdot P_B$. Using these, the Sudakov decomposition of any four vector reads:

$$k^\mu = k^+ n_-^\mu + k^- n_+^\mu + k_T^\mu, \quad (4)$$

where

$$k_T \cdot P_A = k_T \cdot P_B = 0, \quad k_T \cdot k_T = -|\vec{k}_T|^2. \quad (5)$$

The central assumption in our investigations is that the nucleus (or a proton) is probed at small longitudinal momentum transfers compared to the hadron longitudinal momentum. That is, we define longitudinal momentum fractions

$$x_A = \frac{k_1 \cdot P_B}{P_A \cdot P_B}, \quad x_B = \frac{k_2 \cdot P_A}{P_B \cdot P_A}, \quad (6)$$

where k_1 is the momentum transferred to the target A , whereas k_2 is the momentum transferred to the proton target. We assume

$$x_A \ll x_B. \quad (7)$$

These fractions can be also expressed in terms of the final state rapidities y_i and transverse momenta

$$x_A = \frac{1}{\sqrt{s}} (p_{T1} e^{-y_1} + p_{T2} e^{-y_2}), \quad x_B = \frac{1}{\sqrt{s}} (p_{T1} e^{y_1} + p_{T2} e^{y_2}), \quad (8)$$

Therefore, restricting the final states to a large rapidity window and keeping the jet transverse momenta relatively low guarantees the smallness of x_A .

In phenomenological applications, we shall follow the realistic setup of the LHC experiments that measured (or plan to measure) forward dijets in proton-proton and proton-nucleus collisions: ATLAS and ALICE with their planned forward calorimeter FoCal. We shall discuss the kinematic cuts more precisely in Section 4 devoted to phenomenology.

2.2 QCD at high energy

One of the biggest achievements in theoretical developments of perturbative QCD are hard factorization theorems (see [31] for a review). These include the collinear factorization and the TMD factorization, both types proved to all orders in coupling constant α_s and the leading power in the hard scale Q^2 , for few sufficiently inclusive processes. In practice, not only the truncation of perturbation series in α_s is necessary (at present at very low orders), but also the limit $Q^2 \rightarrow \infty$ is rarely adequate. Indeed, when comparing with experimental data, for example for large transverse momenta dijet production [32,33], both a normalization factor (so-called K -factor) is needed, as well as a resummation (parton shower) with the addition of semi-nonperturbative effects (like multiple interactions).

In the collinear factorization or TMD factorization, one encounters powers of logarithms of both x_A and x_B at every perturbative order. Therefore, at very large energies, small transverse momenta, forward production, or a mixture of all of these conditions, the perturbative expansion becomes less reliable. Although within the collinear factorization, it is in principle possible to resum the logarithms of small x (see [34] and references therein), this does not address the two important issues. First, the evolution of the PDFs is always linear, whereas at high energy QCD, one must include the nonlinear effects that will tame the growth of the cross section as required by

the unitarity of the scattering matrix [35]. Second, the collinear factorization neglects higher twist effects (that contribute to the power corrections). For a discussions of higher twists in inclusive DIS and Drell-Yan see *e.g.* [36–41].

Below, we briefly recall the existing approaches that attempt to address the above issues (for an extensive and pedagogical review of high energy QCD see [8]). We focus on the central ideas and main references, skipping the technical details.

Pomeron and The Reggeon Field Theory

Historically, Pomeron – the Regge trajectory with intercept greater than one and vacuum quantum numbers, was introduced in order to explain the growth of the total hadronic cross section with energy. The nature of this quasi-particle is essentially non-perturbative. Together with its parity-odd partner, the Odderon, they constitute a possible effective theory of strong interactions with color singlet degrees of freedom. Typically, their interactions are described by the Euclidean field theory called the Regge field theory [42] (see also [43, 43] and [44, 45]). In its most general form, it includes the multiple Pomeron and Odderon interaction, but in the context of unitarity, one typically studies a truncation to the triple Pomeron vertex.

In perturbative QCD the parity even color singlet state exchanged in the t channel can be made out of two gluons. This leads to the perturbative Pomeron of Balitsky, Fadin, Kuraev and Lipatov (BFKL) [46–49] (for a pedagogical review see *eg.* [50]). The corresponding energy evolution equation of the Pomeron Green function gives the power like behavior of the cross section with energy. The triple Pomeron vertex needed for nonlinear taming of the growth can also be constructed in QCD [51–53]. The difference in the Pomeron intercept derived in perturbative QCD and the one needed to describe for example elastic hadron-hadron scattering leads to a distinction between the hard and the soft Pomeron.

There are numerous applications of the Pomeron calculus to particle production; in particular, there exist several Monte Carlo event generators: PHOJET and DPMJET [54, 55], EPOS [56, 57], SIBYLL [58, 59], QGSJET [60, 61].

Lipatov effective action

The effective building blocks of the diagrams in the BFKL approach are the “reggeized” gluons R and effective interaction vertices $RR \rightarrow g$. The former is characterized by the eikonal coupling to other vertices (due to the high energy approximation) and the “reggeization” factor $(-s)^{\omega(t)}$ appearing due to radiative corrections, where $\omega(t)$ is the perturbative Regge trajectory. The RRg effective vertices are separated in rapidity (the quasi-multi-Regge kinematics).

Stripping off the reggeization factors, the building blocks can be formalized into an effective gauge invariant action [62, 63] that contains both the QCD degrees of freedom, and the reggeized gluon fields A_+ , A_- , that, roughly, by virtue of equations of motions are straight semi-infinite Wilson lines along two light-cone directions P_A and P_B . The vertices are naturally generalized into $RRg \dots g$ vertices, as well as multiple reggeon vertices. For a review see [64] (chapter 11 in [65]).

Using Lipatov’s high energy effective action beyond tree level is rather cumbersome due to double counting between gluon field and composite reggeons, but several results have been obtained (see for example [66–70]). The important feature of that action is that it includes all the necessary ingredients to unitarize the cross section. In particular in [71–74] a relation to the Color Glass Condensate was established and investigated.

High Energy Operator Product Expansion

Consider a projectile, a photon for simplicity, scattering off a hadron in a frame where it is moving slowly. The photon fluctuates into a pair of quarks well before it hits the target and – at high energies – interacts with the target eikonally. In the considered high energy kinematics, the target is made of gluons, that are treated as background field, which shrinks to a shock wave. The quark-antiquark dipole interacts with that shockwave becoming a straight infinite Wilson lines of the background field. Since the scattering cross section is related to the hadronic matrix element of the time ordered product of quark current, effectively, the above picture provides a means of

decomposing the hadronic tensor into products of Wilson lines and the so-called impact factors. This is the essence of the high energy operator product expansion [75]. More precisely

$$\mathcal{T} \{J^\mu(x)J^\nu(y)\} = \int d^2 z_{1T} d^2 z_{2T} \mathcal{I}_2^{\mu\nu}(x, y; \vec{z}_{1T}, \vec{z}_{2T}) \text{Tr} U(\vec{x}_T) U^\dagger(\vec{y}_T) + \dots, \quad (9)$$

where

$$U(\vec{x}_T) = \mathcal{P} \exp \left\{ ig \int dw^+ \hat{A}^-(x_T + w^+) \right\} \quad (10)$$

is the straight infinite Wilson line along the plus light cone direction and fixed transverse position, whereas $\mathcal{I}_2^{\mu\nu}$ is the leading order impact factor. The dots represent the subleading corrections. Similar to the treatment of the ordinary factorization, where the hadronic matrix element is traded to the partonic one when deriving the evolution equation, here it is traded to the matrix element of the background gluon field

$$\langle P_A | \dots | P_A \rangle \rightarrow \langle \dots \rangle. \quad (11)$$

The distinction between the background field and the projectile is related to the rapidity; formally the matrix elements depend on the rapidity cutoff. This dependence is explicitly introduced when regulating the rapidity divergence appearing when considering perturbative correction. However, a perturbative gluon interacting with the shock wave generates an adjoint Wilson line that gives a product of four fundamental Wilson lines. The evolution of this four-point correlator generates in turn further higher point correlators. Therefore the resulting evolution equation is not closed and consists of a tower of products of an increasing number of Wilson lines, known as the Balitsky hierarchy. However, at the large N_c limit, the hierarchy is terminated and one obtains a single evolution equation for the product of two Wilson lines, the so-called *dipole* amplitude

$$N(\vec{x}_T, \vec{y}_T; \eta) = 1 - \frac{1}{N_c} \langle \text{Tr} U(\vec{x}_T) U^\dagger(\vec{y}_T) \rangle, \quad (12)$$

where η is the implicit rapidity cutoff. The evolution equation [75] reads

$$\frac{\partial}{\partial \eta} N(\vec{x}_T, \vec{y}_T; \eta) = \frac{\alpha_s N_c}{2\pi} \int d^2 z_T \frac{(\vec{x}_T - \vec{y}_T)^2}{(\vec{x}_T - \vec{z}_T)^2 (\vec{y}_T - \vec{z}_T)^2} \left\{ N(\vec{x}_T, \vec{z}_T; \eta) + N(\vec{y}_T, \vec{z}_T; \eta) - N(\vec{x}_T, \vec{y}_T; \eta) - N(\vec{x}_T, \vec{z}_T; \eta) N(\vec{z}_T, \vec{y}_T; \eta) \right\}. \quad (13)$$

It was also obtained independently in [76] using the Mueller dipole approach [77] and is therefore called the Balitsky-Kovchegov (BK) equation.

Typically one introduces new variables, the dipole size

$$\vec{r}_T = \frac{\vec{x}_T - \vec{y}_T}{2}, \quad (14)$$

and the impact parameter

$$\vec{b}_T = \frac{\vec{x}_T + \vec{y}_T}{2}. \quad (15)$$

The usual treatment of that equation assumes an infinite target and thus neglects the impact parameter dependence [78–86], but solutions with impact parameter are also known, see [87] and the following works, including [88–93].

Let us finally mention the huge progress in controlling next-to-eikonal corrections, see [94–100], as well as the development of the next-to-leading order BK equation [101–106].

Color Glass Condensate

The High Energy Operator Product expansion does provide the evolution equation but does not allow for the calculation of the non-perturbative correlators itself.

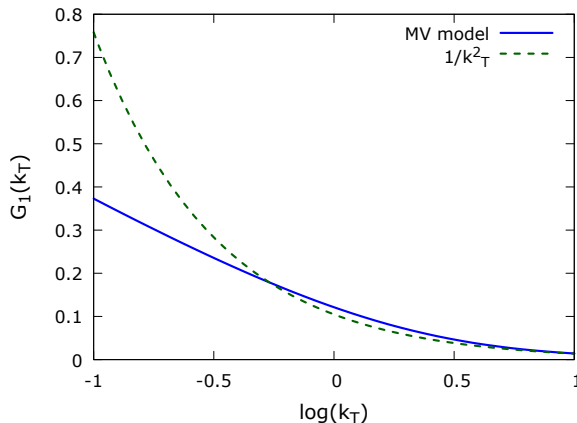


Figure 2: Gluon saturation phenomenon in the MV model. The perturbative behaviour $\sim 1/k_T^2$ is tamed at $k_T \sim Q_s$, with Q_s increasing with energy.

On the other hand, the effective theory of high energy QCD – the Color Glass Condensate (CGC) is a convenient framework to approach both the evolution and averages of Wilson lines in the background color field (for a review see for example [5]).

It is convenient to review now a famous model of large nucleus – the McLerran-Venugopalan (MV) model [107, 108]. Assume we view a large nucleus with a large number of nucleons in a frame where it is moving with a very large velocity. In that boosted frame, large x partons are localized in one of the light-cone directions and can be considered as color sources for the classical Yang-Mills fields. These sources are some, apriori unknown, distributions in the transverse plane $\rho_a(x_T)$ and are considered independent within the large nucleus because there are large numbers of nucleons inside. One can solve the Yang-Mills equation for such configuration to obtain the gluon “wee” fields. In order to compute observables, one needs to average over the color sources. For example, a basic quantity to consider is the particle number density with the generic definition

$$\frac{dn}{d^3\mathbf{k}} \sim \langle P_A | \tilde{A}_b^i(y^+, \mathbf{k}) \tilde{A}_b^i(y^+, -\mathbf{k}) | P_A \rangle, \quad (16)$$

where \tilde{A}_b^i are partially Fourier transformed gauge fields, $\mathbf{k} = (k^+, \vec{k}_T)$ is a three-vector conjugate to $\mathbf{y} = (y^-, \vec{y}_T)$. We have assumed here that the large boost is in the light cone “plus” direction. In the MV model, the hadronic matrix element of the gluon field correlator is traded to

$$\langle A_b^i(\mathbf{y}) A_b^i(\mathbf{z}) \rangle_x = \int [d\rho] \mathcal{W}_x[\rho] A_b^i[\rho](\mathbf{y}) A_b^i[\rho](\mathbf{z}), \quad (17)$$

where the averaging is over the color sources in the functional sense. \mathcal{W}_x is the functional weight for random color sources, which in the MV model is a Gaussian. Direct computation of the above gluon distribution leads to the so-called Weizsacker-Williams (WW) gluon distribution [109, 110]. Interestingly, despite it being the most basic quantity in the MV model it is not the easiest one to compute nor can it be probed in the simplest scattering processes. Rather, as we discuss later, the quantities that appear for example in inclusive DIS are correlators of Wilson lines. The WW gluon distribution can be approximated as

$$G_1(k_T) \sim \int d^2r_T \frac{e^{-i\vec{k}_T \cdot \vec{r}_T}}{|\vec{r}_T|} \left[1 - \exp \left(-\frac{1}{4} \alpha_s N_c \mu_A |\vec{r}_T|^2 \log \frac{1}{r_T \Lambda_{\text{QCD}}} \right) \right], \quad (18)$$

where μ_A is the average color charge per unit transverse area per color. The saturation phenomenon is visible in the above distribution as follows. If the two-point correlator (16) was an ordinary perturbative correlator it would behave like $\sim 1/k_T^2$; this behavior leads to the power-like growth of the gluon distribution. It turns out that (18) behaves like $\sim 1/k_T^2$ in the perturbative domain

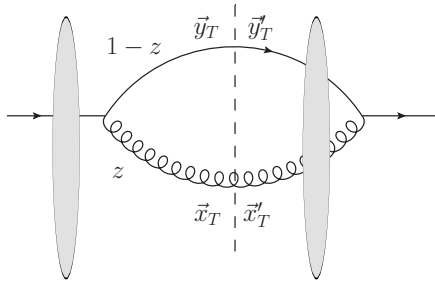


Figure 3: Scattering of a color dipole $q \rightarrow qq$ off a nuclear target in CGC. The shaded ellipses symbolize the color field of a nucleus. This particular diagram corresponds to a contribution, where in the amplitude the incoming quark scatters off the color field of the nucleus before the splitting, while in the amplitude conjugate both gluon and a quark scatter after splitting. Particles scattering off the color field of the nucleus gain infinite straight Wilson line along the light cone, in their respective representations.

(large k_T), but at small k_T it behaves like $\frac{1}{\alpha_s} \log \frac{Q_s^2}{k_T^2}$, where Q_s is the scale at which the suppression happens, called the *saturation scale* (see Fig. 2). This dynamical scale depends on x (through the evolution) and increases with decreasing x .

The subscript x in the functional weight \mathcal{W}_x denotes a longitudinal cutoff between the sources and the “wee” partons. Decreasing the cutoff produces new color sources and thus the Gaussian distribution gets distorted. The CGC high energy effective theory predicts the evolution equation of \mathcal{W}_x in x . It is the so-called Jalilian-Marian-Iancu-McLerran-Weigert-Leonidov-Kovner (JIMWLK) equation [111–116] and has the following general form

$$\frac{d\mathcal{W}_x[\rho]}{d \ln x} = -H_{\text{JIMWLK}} \left[\rho, \frac{\delta}{\delta \rho} \right] \mathcal{W}_x[\rho], \quad (19)$$

where H_{JIMWLK} is the so-called JIMWLK Hamiltonian (we skip its exact form here). It gives a nonlinear evolution of \mathcal{W}_x and in turn also a nonlinear evolution of any gauge field-dependent quantity due to the averaging procedure in ρ . These equations are consistent with the Balitsky hierarchy mentioned earlier, therefore it is often called B-JIMWLK equation.

2.3 Small- x Improved TMD (ITMD) factorization

In this section, we shall review the formalism that is suitable for phenomenological studies of forward jet production processes at moderate transverse momenta. The formalism lies at the intersection of the two aspects of QCD that in the past were rarely overlapping and, essentially, were exercised by distinct communities. One is the high energy scattering reviewed in the previous Section and the other is the hard factorization theorems, in particular the TMD factorization (see eg. [31] for a review).

Dijet production in dilute-dense collisions

We start with a CGC description of a scattering of a proton or a photon off a nuclear target to produce two partons. The basic assumption here is that, in the case of the proton projectile, it is dilute, that is the partons extracted from the projectile are moderate x partons. With that assumption, we can treat the scattering of color dipoles, such as $\gamma \rightarrow q\bar{q}$, $q \rightarrow qq$, etc., off a color field of a nucleus. This is the essence of the dilute-dense (or hybrid) approach which, as explained in Section 2.1, is kinematically well suited to study forward jets [117].

Consider, as an example, the scattering of a $q \rightarrow qq$ color system off a nuclear target (Fig. 3). In the shock wave approximation, the interaction with the color field of the nucleus can take place either before the quark splits or after. For example, in Fig. 3 the scattering takes place before the splitting in the amplitude and after the splitting in the amplitude conjugate. Each colored particle

gains a nonabelian phase when scattering, given by the Wilson line

$$U_R(\vec{x}_T) = \mathcal{P} \exp \left\{ ig \int_{-\infty}^{+\infty} dx^- A_a^+(x^-, \vec{x}_T) T_R^a \right\}, \quad (20)$$

where the generator T_R^a is in the fundamental representation ($R = F$) for a quark or in the adjoint representation ($R = A$) for a gluon. The cross section for the scattering of that system can be written as [22]

$$\begin{aligned} \frac{d\sigma_{qA \rightarrow qg}}{d^2p_{1T} d^2p_{2T} dy_1 dy_2} &\sim \int \frac{d^2x_T}{(2\pi)^2} \frac{d^2x'_T}{(2\pi)^2} \frac{d^2y_T}{(2\pi)^2} \frac{d^2y'_T}{(2\pi)^2} e^{-i\vec{p}_{1T} \cdot (\vec{x}_T - \vec{x}'_T)} e^{-i\vec{p}_{2T} \cdot (\vec{y}_T - \vec{y}'_T)} \\ &\psi_q^*(z, \vec{x}'_T - \vec{y}'_T) \psi_q(z, \vec{x}_T - \vec{y}_T) \left\{ S_x^{(4)}(\vec{y}_T, \vec{x}_T, \vec{y}'_T, \vec{x}'_T) \right. \\ &- S_x^{(3)}(\vec{y}_T, \vec{x}_T, (1-z)\vec{y}'_T + z\vec{x}'_T) - S_x^{(3)}((1-z)\vec{y}_T + z\vec{x}_T, \vec{y}'_T, \vec{x}'_T) \\ &\left. - S_x^{(2)}((1-z)\vec{y}_T + z\vec{x}_T, (1-z)\vec{y}'_T + z\vec{x}'_T) \right\}, \quad (21) \end{aligned}$$

where $\psi_q(z, \vec{x}_T)$ is the wave function of the dipole, with z being a fraction of the incoming quark momentum taken by a gluon. This wave function can be computed in perturbative QCD. The quantities in the curly bracket correspond to the color averages of the Wilson lines:

$$S_x^{(2)}(\vec{x}_T, \vec{y}_T) = \frac{1}{N_c} \left\langle \text{Tr} U_F(\vec{x}_T) U_F^\dagger(\vec{y}_T) \right\rangle_x \quad (22)$$

$$S_x^{(3)}(\vec{x}_T, \vec{y}_T, \vec{z}_T) = \frac{1}{C_F N_c} \left\langle \text{Tr} \left\{ U_F^\dagger(\vec{z}_T) t^a U_F(\vec{x}_T) t^b \right\} U_A^{ab}(\vec{y}_T) \right\rangle_x \quad (23)$$

$$S_x^{(4)}(\vec{x}_T, \vec{y}_T, \vec{x}'_T, \vec{y}'_T) = \frac{1}{C_F N_c} \left\langle \text{Tr} \left\{ U_F(\vec{x}_T) U_F^\dagger(\vec{x}'_T) t^b t^a \right\} \left\{ U_A(\vec{y}_T) U_A^\dagger(\vec{y}'_T) \right\}^{ab} \right\rangle_x. \quad (24)$$

The above correlators depend on x through the B-JIMWLK equations. In practice, one often uses the Gaussian approximation [118], which states that the color source distribution stays Gaussian throughout the evolution. This allows us to compute the evolution of correlators in closed form.

In order to compute the differential cross section for dijet production in proton-nucleus scattering in the above setup, one needs to find the remaining color dipole contributions [22, 119] and convolute the parton-nucleus cross section with the ordinary collinear PDFs.

The CGC formulation of the dilute-dense scattering provides the high-energy description of the jet production at both small transverse momenta p_T of jets and moderate (at very large p_T one should switch the approach from leading energy to leading power in the hard scale). The drawback of the above approach, in addition to being hard to generalize and implement in a Monte Carlo code, is that the perturbative information is contained not only in the color dipole wave function but also in the correlators. As we discuss later, in certain limits this information can be extracted and combined with the dipole wave function to obtain the hard matrix elements, similar to those known from hard factorization.

At the end, let us mention a huge progress in computing higher orders in particle production within the CGC framework. The NLO results for single inclusive jets are available already for some time [120–122], also with resolutions of the “negative cross section” problem [123–126]. Further, there are NLO computations for inclusive DIS [19, 127], also with heavy quarks [128, 129], dijets in DIS [130–132], vector meson production [133, 134], dijet and dihadron hadroproduction [135–137]. Higher multiplicity LO computations in CGC include dijet and photon production [138], trijets [139] and trijets in photoproduction [140].

High Energy (or k_T) factorization

Usually, the high energy factorization (HEF) (or k_T -factorization) refers to a description of particle production at asymptotically high energies in terms of “unintegrated” PDFs that undergo the

BFKL [141, 142] or CCFM [143, 144] evolution. More precisely, within HEF the cross section for a multi-jet production in a collision of two hadrons can be written as

$$d\sigma_{AB} \left(P_A, P_B; p_1^{(J)}, \dots, p_n^{(J)} \right) = \int dx_A dx_B \int d^2 k_{1T} d^2 k_{2T} \mathcal{F}_{g/A} \left(x_A, |\vec{k}_{1T}| \right) \mathcal{F}_{g/B} \left(x_B, |\vec{k}_{2T}| \right) d\hat{\sigma}_{RR} \left(x_A P_A + k_{1T}, x_B P_B + k_{2T}; p_1^{(J)}, \dots, p_n^{(J)}; \mu \right), \quad (25)$$

where $\mathcal{F}_{g/H}$ are unintegrated gluon distributions defined as

$$\mathcal{F}_{g/H} \left(x, |\vec{k}_T| \right) = \int \frac{d^2 p_T}{2\pi} \frac{\Phi_H(\vec{p}_T)}{|\vec{p}_T|^2} \mathcal{G} \left(\vec{p}_T, \vec{k}_T; x \right), \quad (26)$$

where Φ_H is the non-perturbative impact factor of a hadron and \mathcal{G} is the BFKL Green's function. At leading order, the partonic cross section in (25) reads

$$d\hat{\sigma}_{RR}^{(0)} \left(k_1, k_2; p_1^{(J)}, \dots, p_n^{(J)} \right) = \frac{1}{2x_A x_B s} |\bar{V}_{RR \rightarrow P \dots P}(k_1, k_2; p_1, \dots, p_n)|^2 F \left(\{p_i\}, \{p_i^{(J)}\} \right) d\Gamma_n(\{p_i\}), \quad (27)$$

where $V_{RR \rightarrow P \dots P}$ (the bar denotes the usual spin/color summation and averaging) is the suitably normalized tree-level $RR \rightarrow P \dots P$ vertex to produce n partons (jets), with R being reggeon states understood as fields from the high energy Lipatov's action (*i.e.* without the “reggeization” factors), while P being on-shell quarks or gluons. Above, $d\Gamma_n$ is ordinary on-shell phase space and F is a jet function that implements the cuts. The momenta of reggeons are

$$k_1^\mu = x_A P_A^\mu + k_{1T}^\mu \quad k_2^\mu = x_B P_B^\mu + k_{2T}^\mu. \quad (28)$$

Notice that they are off-shell $k_{1,2}^2 = -|\vec{k}_{T1,2}|^2$ and lack one of the light-cone components, due to the high energy approximations.

In the original work on HEF in heavy quark production [142] the partonic cross section (27) was expressed in terms of off-shell amplitude to produce heavy quark pair, with initial gluons having momenta (28) and projected onto P_A and P_B (eikonal coupling). In that simple case, it turns out that the amplitude calculated in terms of ordinary diagrams is gauge invariant, despite the initial gluons being off-shell. In practical applications, it proves to be very convenient to stick to that logic also for more complicated processes, instead of using Lipatov's effective action. Indeed, it is possible to define off-shell gauge invariant amplitude for arbitrary processes. In addition to ordinary Feynman diagrams (with off-shell space-like gluons), one needs “gauge restoring” contributions. Those additional diagrams can be reconstructed for example by the “embedding” method [145], where an off-shell process is embedded in an on-shell process with special kinematics of the auxiliary quarks or gluons. This method was automatized for arbitrary Standard Model tree level process in the KATIE Monte Carlo discussed in Section 3¹. Also, other methods suitable for automatization were also developed [147–150]. In Fig. 4 we illustrate one of the methods.

In the context of forward jets, one can apply similar considerations to the hybrid approach explained before. Namely, when, say, x_B is moderate and not small, one should extract partons from collinear PDF rather than unintegrated PDF undergoing BFKL evolution. This was discussed in [151] and the corresponding HEF formula reads

$$d\sigma_{AB}^{\text{forward}} \left(P_A, P_B; p_1^{(J)}, \dots, p_n^{(J)} \right) = \sum_a \int dx_A dx_B \int d^2 k_T f_{a/B}(x_B, \mu) \mathcal{F}_{g/A} \left(x_A, |\vec{k}_T|; \mu \right) d\hat{\sigma}_{ag^*} \left(x_B P_B, x_A P_A + k_T; p_1^{(J)}, \dots, p_n^{(J)}; \mu \right), \quad (29)$$

¹The first Monte Carlo implementation of the High Energy Factorization was achieved within the CASCADE framework [146]

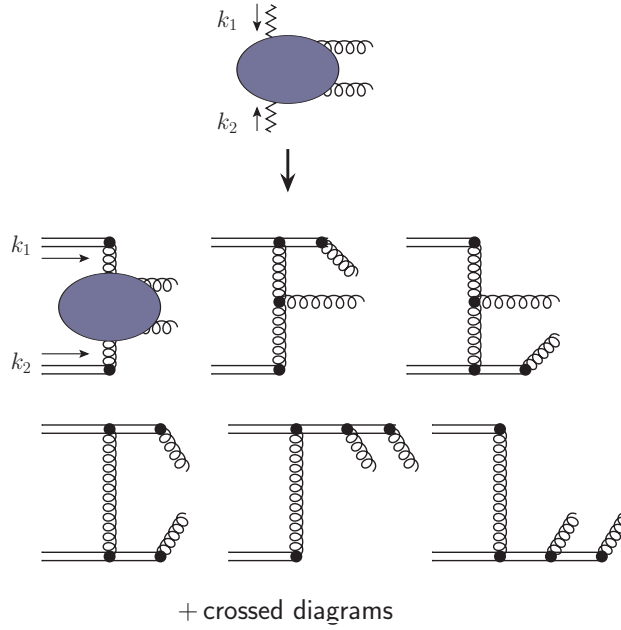


Figure 4: Off-shell gauge invariant amplitude (upper blob – the zigzag lines represent off-shell gauge invariant gluons) can be constructed by promoting a single off-shell gluon coupled eikonally to a straight infinite Wilson line along corresponding hadron momenta P_A or P_B . Here we show diagrams for the production of two gluons at tree level. The double line represents the momentum space Wilson line along P_A (for the top line) and P_B (for the bottom line). Gluons couple to these Wilson lines via $igt^a p_{A(B)}^\mu$ and the double-line propagators have form $i/(k \cdot p_{A(B)} + i\epsilon)$. Only planar diagrams are shown. The blob represents all possible connections of gluons via standard vertices.

where we have explicitly denoted the fact that the partonic cross section is constructed from amplitude with one off-shell (gauge invariant) gluon. Above $f_{a/B}$ is the collinear PDFs for parton a (quark or gluon) in hadron B .

Let us now refocus our attention to the dijet case. It turns out that the k_T -factorization formula with proper gauge invariant off-shell amplitudes can be retrieved from the CGC expressions discussed before [30, 119]. In the dilute limit, which corresponds to $|\vec{k}_T| \gg Q_s$, one can neglect the multiple scattering off the target. This means that the triple and quadrupole operators $S^{(3)}$, $S^{(4)}$ can be expressed only in terms of the dipole $S^{(2)}$. In that limit, one obtains for the $q \rightarrow qg$ dipole scattering

$$\frac{d\sigma_{pA \rightarrow qg}}{d^2p_{1T} d^2p_{2T} dy_1 dy_2} = x_B f_{q/B}(x_B, \mu^2) \mathcal{F}_{g/A}(x_A, |\vec{k}_T|) \frac{\alpha_s (1-z)(1+(1-z)^2)}{2\pi |\vec{p}_{1T}|^2 |\vec{p}_{2T}|^2} \left[1 + \frac{(1-z)^2 |\vec{p}_{T1}|^2}{|\vec{P}_T|^2} - \frac{1}{N_c^2} \frac{z^2 |\vec{p}_{T2}|^2}{|\vec{P}_T|^2} \right], \quad (30)$$

where

$$\vec{P}_T = (1-z)\vec{p}_{1T} + z\vec{p}_{2T} \quad (31)$$

and the unintegrated gluon distribution is related to the average of the weak field limit of the CGC dipole operator as follows

$$\mathcal{F}_{g/A}(x, |\vec{k}_T|) = \frac{N_c}{\alpha_s (2\pi)^3} \int d^2y_T d^2z_T e^{-i\vec{k}_T \cdot (\vec{y}_T - \vec{z}_T)} \nabla_{\vec{y}_T - \vec{z}_T}^2 \left[1 - S_x^{(2)\text{weak}}(\vec{y}_T, \vec{z}_T) \right]. \quad (32)$$

The hard factor obtained above turns out to be exactly the off-shell gauge invariant amplitude.

TMD factorization

Formally, the TMD factorization is the leading power (in the hard scale μ^2) factorization of a cross section into TMD dependent PDFs and hard factors, that to leading power are on-shell (for a review see [31] and [152, 153]). This factorization does not resum the large small- x logarithms, therefore becomes unreliable at very high energies. Moreover, formally it does not hold for processes we are interested in. However, the formalism provides sturdy theoretical definitions of the TMD gluon distributions that, as it turns out, can be matched to the CGC correlators.

In TMD factorization, gluon distribution is given by the Fourier transform of the bilocal matrix element of the gluon field strength tensor

$$\mathcal{F}_{C_1 C_2}(x, |\vec{k}_T|) = 2 \int \frac{d\xi^- d^2 \xi_T}{(2\pi)^3 P_A^+} e^{ixP_A^+ \xi^- - i\vec{k}_T \cdot \vec{\xi}_T} \langle P_A | \text{Tr} \hat{F}^{j+}(\xi^-, \vec{\xi}_T, 0) \mathcal{U}_{C_1} \hat{F}^{j+}(0) \mathcal{U}_{C_2} | P_A \rangle, \quad (33)$$

where $\hat{F}^{j+} = F_a^{j+} t^a$ is the gluon field strength tensor; the two operators are displaced in both the light cone and transverse direction (unlike in the collinear PDF, where the displacement is only along the light cone). The bilocal operator would not be gauge invariant, therefore the proper general definition requires gauge links \mathcal{U}_{C_1} and \mathcal{U}_{C_2} (here everything is in the fundamental representation) that connect the two space-time points. There is also a possibility of the double-trace over the fundamental representation (see below). We consider here only the unpolarized case, therefore the transverse index j is summed over. The TMD gluon distributions are connected to a partonic process by virtue of factorization. Since we consider gauge theory, there are multiple soft and collinear gluons that can be connected to various places in the diagrams. The definition given above corresponds to the bare operator. In perturbation theory, it contains UV and rapidity divergences that, for some processes, can be removed order-by-order by the operator renormalization and by (part of) the soft factor accumulating soft gluons. This gives the hard scale and rapidity evolution of the TMD PDFs. The collinear gluons (collinear to the target hadron) can be resummed into the Wilson lines \mathcal{U}_{C_1} and \mathcal{U}_{C_2} . As can be easily understood, the form of these Wilson lines depends on the actual hard process (its color flow). In [154] a general procedure of determining these Wilson lines via resummation of collinear gluons was given. It turns out, that they can become quite complicated for colored partonic processes, see for example [155]. In Table 1 we collect the operators relevant for the dijet production. The notation $\mathcal{F}_{gg}^{(i)}$ and $\mathcal{F}_{qg}^{(i)}$ corresponds to TMD PDFs that appear for incoming gluons (the ‘‘gg’’ subscript) or quark-gluon system (the ‘‘qg’’ subscript), and various color flows (the (i) superscript). The Wilson lines $\mathcal{U}^{[\pm]}$ are defined as

$$\mathcal{U}^{[-]} = \left[(\xi^-, \vec{\xi}_T, 0), (-\infty, \vec{\xi}_T, 0) \right] \left[(-\infty, \vec{\xi}_T, 0), (-\infty, \vec{0}_T, 0) \right] \left[(-\infty, \vec{0}_T, 0), (0, \vec{0}_T, 0) \right], \quad (34)$$

which is the past-pointing staple-like gauge link and

$$\mathcal{U}^{[+]} = \left[(\xi^-, \vec{\xi}_T, 0), (+\infty, \vec{\xi}_T, 0) \right] \left[(+\infty, \vec{\xi}_T, 0), (+\infty, \vec{0}_T, 0) \right] \left[(+\infty, \vec{0}_T, 0), (0, \vec{0}_T, 0) \right] \quad (35)$$

is the future pointing ‘‘staple’’, see Fig. 5. The square brackets above $[x, y]$ is a standard notation for segments of straight gauge link between the points x and y . Out of two staples it is possible to make a Wilson loop

$$\mathcal{U}^{[\square]} = \mathcal{U}^{[-]\dagger} \mathcal{U}^{[+]}. \quad (36)$$

The relation of the field theoretical definitions of TMD PDFs and small- x QCD has been a subject of intense work, see for example [156–167]. In the context of forward dijet production, we are interested in the small- x limit of the TMD gluon distributions. This is achieved by literally taking the limit $x_A \rightarrow 0$ in the definitions. On the other hand, one can consider the leading power limit of the CGC expressions (21). This leads to the identification of the TMD gluon distributions and the leading terms in the gradient expansions of the CGC correlators [157]. For example

$$\mathcal{F}_{gg}^{(1)} = \frac{1}{\pi\alpha_s} \int \frac{d^2 x_T d^2 y_T}{2\pi^3} e^{-i\vec{k}_T \cdot (\vec{x}_T - \vec{y}_T)} \left\langle \text{Tr} \partial_j U_F(\vec{y}_T) \partial_j U_F^\dagger(\vec{x}_T) \right\rangle_x, \quad (37)$$

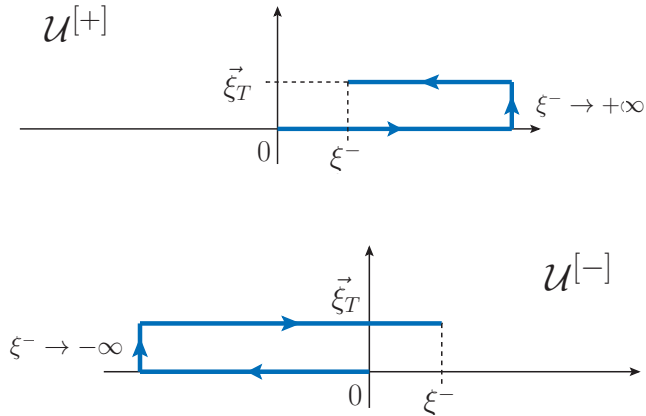


Figure 5: The shape of the “staple-like” gauge links $\mathcal{U}^{[+]}$ and $\mathcal{U}^{[-]}$. The horizontal axis represents the light-cone minus direction, the vertical axis symbolizes the transverse displacement. The transverse pieces are placed at $+\infty$ and $-\infty$, respectively.

$$\mathcal{F}_{qg}^{(2)} = -\frac{1}{\pi\alpha_s N_c} \int \frac{d^2 x_T d^2 y_T}{2\pi^3} e^{-i\vec{k}_T \cdot (\vec{x}_T - \vec{y}_T)} \left\langle \text{Tr} \left\{ \partial_j U_F(\vec{x}_T) U_F^\dagger(\vec{y}_T) \partial_j U_F^\dagger(\vec{y}_T) U_F(\vec{x}_T) \right\} \right. \\ \left. \times \text{Tr} \left\{ U_F(\vec{y}_T) U_F^\dagger(\vec{x}_T) \right\} \right\rangle_x, \quad (38)$$

that is, the $\mathcal{F}_{qg}^{(1)}$ is identified with the expansion of the dipole operator. For the complete list of similar relations for other TMDs see [157, 168]. Ultimately, in the leading power limit, the CGC formula for the $qg \rightarrow qg$ contribution can be written as

$$\frac{d\sigma_{pA \rightarrow qg+X}}{d^2 P_T d^2 k_T dy_1 dy_2} = \frac{1}{(x_A x_B s)^2} x_B f_{q/B}(x_B, \mu^2) \sum_{i=1}^2 \mathcal{F}_{qg}^{(i)}(x_A, |\vec{k}_T|) \mathcal{H}_{qg \rightarrow qg}^{(i)}, \quad (39)$$

where s is the hadronic center of mass energy and $\mathcal{H}_{qg \rightarrow qg}^{(i)}$ are on-shell hard factors corresponding to the two independent color flows. They read

$$\mathcal{H}_{qg \rightarrow qg}^{(1)} = \alpha_s^2 (\hat{u}^2 + \hat{s}^2) \left(-\frac{\hat{u}}{2\hat{s}\hat{t}^2} + \frac{1}{2N_c^2} \frac{1}{\hat{s}\hat{u}} \right), \quad (40)$$

$$\mathcal{H}_{qg \rightarrow qg}^{(2)} = \alpha_s^2 (\hat{u}^2 + \hat{s}^2) \left(-\frac{\hat{s}}{2\hat{u}\hat{t}^2} \right), \quad (41)$$

where \hat{s} , \hat{t} , \hat{u} are the Mandelstam variables.

In collinear LO factorization, both TMD gluon distributions would be replaced by the collinear gluon PDFs and the above hard factors would be added. It is easy to check that the sum corresponds to the known on-shell hard factor for $qg \rightarrow qg$ process. The list of all hard factors for all subprocesses beyond the large N_c limit is given in [148].

In the end, let us mention progress in establishing the CGC-leading power TMD factorization correspondence. In [155] the Authors explicitly obtained the structure of all TMD operators corresponding to five and six colored parton processes. In [140] the TMD factorization limit was studied for three jet production in CGC. Finally, in [137] the TMD factorization was studied in the context of dijet production in photoproduction at NLO.

ITMD and resummation of kinematic twists

It is important to stress, that the TMD factorization in dilute-dense collisions, despite being leading power, does take into account gluon saturation. First, notice that the leading power means here

$\mathcal{F}_{C_1 C_2}$	$\mathcal{F}_{gg}^{(1)}$	$(*)\mathcal{F}_{gg}^{(2)}$	$\mathcal{F}_{gg}^{(3)}$	$\mathcal{F}_{gg}^{(4)}$	$\mathcal{F}_{gg}^{(5)}$	$\mathcal{F}_{gg}^{(6)}$
\mathcal{U}_{C_1}	$\frac{\text{Tr}\mathcal{U}^{[\square]\dagger}}{N_c}\mathcal{U}^{[-]\dagger}$	$\mathcal{U}^{[\square]\dagger}$	$\mathcal{U}^{[+]\dagger}$	$\mathcal{U}^{[-]\dagger}$	$\mathcal{U}^{[\square]\dagger}\mathcal{U}^{[+]\dagger}$	$\frac{\text{Tr}\mathcal{U}^{[\square]\dagger}}{N_c}\mathcal{U}^{[+]\dagger}$
\mathcal{U}_{C_2}	$\mathcal{U}^{[+]}$	$\mathcal{U}^{[\square]}$	$\mathcal{U}^{[+]}$	$\mathcal{U}^{[-]}$	$\mathcal{U}^{[\square]}\mathcal{U}^{[+]}$	$\frac{\text{Tr}\mathcal{U}^{[\square]}}{N_c}\mathcal{U}^{[+]}$

$\mathcal{F}_{C_1 C_2}$	$\mathcal{F}_{gg}^{(1)}$	$\mathcal{F}_{gg}^{(2)}$
\mathcal{U}_{C_1}	$\mathcal{U}^{[-]\dagger}$	$\mathcal{U}^{[+]\dagger}$
\mathcal{U}_{C_2}	$\mathcal{U}^{[+]}$	$\frac{\text{Tr}\mathcal{U}^{[\square]}}{N_c}\mathcal{U}^{[+]}$

Table 1: Gauge links \mathcal{U}_{C_1} and \mathcal{U}_{C_2} in terms of the “staple-like” Wilson lines contributing to TMD gluon distributions that are coupled to independent color flows of $gg \rightarrow gg$ and $gg \rightarrow q\bar{q}$ (upper table) and $gg \rightarrow gg$ (lower table) processes. The operators in the column marked with a star * should be traced with the gluon field strength tensor independently.

$k_T \ll P_T$. The saturation scale is not neglected and is of the order of k_T . Second, the leading twist TMD gluon distribution is considered in the strict high energy limit and they still can undergo nonlinear evolution, even at leading twist (for an interesting discussion of two types of saturation see [169]). To summarize, the dilute-dense TMD factorization is suitable when the transverse momenta of dijets are rather large and we are interested in the back-to-back dijet region. For very large transverse momenta of the jets, the highest scale is not given by the energy but the hard scale and one should switch the framework to the collinear factorization.

The main limitation of the dilute-dense TMD factorization is that it works only in the back-to-back region. In dijet studies, especially at small x , dijet azimuthal correlations are the most important observables and can be measured over a wide range of the azimuthal angle. Therefore, it is essential to account not only for jet correlations but also decorrelations. A related issue is that of the transverse momentum conservation. In the TMD factorization, the transverse momentum k_T of the gluon scattered (or extracted) from the target nucleus enters only TMD gluon distributions, and not the hard process. This complicates for example Monte Carlo realization of such an approach.

It turns out, that, in practical terms, it is actually quite easy to improve the dilute-dense TMD factorization. The hard factors have to take into account power corrections due to the transverse momentum of the incoming gluon. This is uniquely realized in the high energy limit by promoting the on-shell hard factors to the gauge invariant off-shell ones, following the rules described in the part devoted to HEF. This procedure was described in detail in [148], where also off-shell gauge invariant hard factors are calculated for all channels and color flows. A proof and proper interpretation within the CGC was later given in [170]. First, a formal distinction between kinematic and genuine twist is made. The genuine twist counting can be simply understood as counting gluon operators in the TMD matrix element (but not the Wilson lines), for example, an operator with two strength field tensors corresponds to twist two and two-body contribution. The kinematic twists are power corrections in k_T to the n -body process and come from the hard matrix element. In [170] a resummation of the kinematic twists was performed for the two-body contributions, showing that the resulting hard factors indeed correspond to the off-shell gauge invariant hard factors.

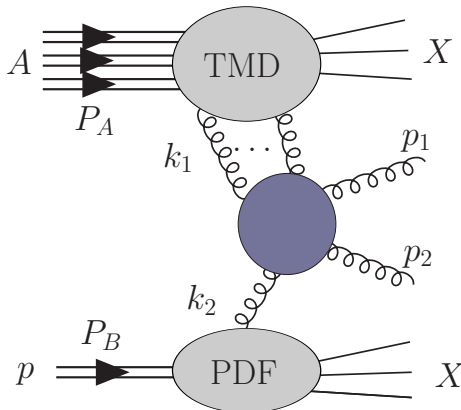


Figure 6: The ITMD factorization (pure gluon channel) of the p+A dijet cross section into TMD PDF (upper blob), the collinear PDF (lower blob) and the off-shell hard part (center blob). Since the exchanged momentum between the upper blob and the center is off-shell, multiple eikonal gluon exchanges are required to maintain the gauge invariance. In ITMD factorization, these gluons do not increase the genuine twist of the TMD operator. The TMD distribution is given by a certain linear combination of the operators listed in Table 1.

Before we review the dilute-dense improved TMD (ITMD) factorization framework, let us first comment, that when determining the TMD gluon distribution functions it is important to work with gauge invariant subset of diagrams and not the individual ones. The systematic way of doing that in small- x physics was suggested in [148], where a decomposition of an amplitude into color-ordered amplitudes was used. The color-ordered amplitudes [171] are gauge invariant, but contain only planar diagrams and correspond to the different ordering of the external partons. Each color-ordered amplitude comes with a color structure, for which the TMD operator can be determined. It is then usually given as some combination of the basic operators build from $\mathcal{U}^{[\pm]}$ Wilson lines, but corresponds to the gauge invariant hard factor. The ITMD framework given below was formulated with that feature in mind.

The ITMD factorization formula, accounting for all channels, reads

$$\frac{d\sigma_{pA \rightarrow JJ+X}}{d^2P_T d^2k_T dy_1 dy_2} = \frac{\alpha_s^2}{(x_A x_B s)^2} \sum_{a,c,d} x_B f_{a/B}(x_B, \mu^2) \sum_{i=1}^2 K_{ag^* \rightarrow cd}^{(i)}(\vec{k}_T) \Phi_{ag \rightarrow cd}^{(i)}(x_A, |\vec{k}_T|) \frac{1}{1 + \delta_{cd}}, \quad (42)$$

where $K_{ag^* \rightarrow cd}^{(i)}(\vec{k}_T)$ are off-shell gauge invariant hard factors and $\Phi_{ag \rightarrow cd}^{(i)}(x_A, |\vec{k}_T|)$ are the corresponding TMD gluon distributions. We collect them in Table 2. They are expressed in terms of the ordinary Mandelstam variables, as well as “modified” Mandelstam variables. The former read explicitly

$$\hat{s} = (k_1 + k_2)^2 = (p_1 + p_2)^2 = \frac{|\vec{P}_T|^2}{z(1-z)}, \quad (43a)$$

$$\hat{t} = (p_2 - k_1)^2 = (p_1 - k_2)^2 = -\frac{|\vec{p}_{2T}|^2}{1-z}, \quad (43b)$$

$$\hat{u} = (p_1 - k_1)^2 = (p_2 - k_2)^2 = -\frac{|\vec{p}_{1T}|^2}{z}, \quad (43c)$$

where the incoming momenta are

$$k_1 = x_A P_A + k_T, \quad k_2 = x_B P_B \quad (44)$$

and

$$z = \frac{p_1^+}{p_1^+ + p_2^+} \quad \text{and} \quad \vec{P}_T = (1-z)\vec{p}_{1T} - z\vec{p}_{2T}. \quad (45)$$

They sum up to $\hat{s} + \hat{t} + \hat{u} = -|\vec{k}_T|^2$. The “modified” Mandelstam variables take into account only the longitudinal component of the off-shell initial state k_1 and read

$$\bar{s} = (x_A P_A + k_2)^2 = \frac{|\vec{P}_T|^2}{z(1-z)} + |\vec{k}_T|^2 = x_A x_B s, \quad (46a)$$

$$\bar{t} = (p_2 - x_A P_A)^2 = -z\bar{s}, \quad (46b)$$

$$\bar{u} = (p_1 - x_A P_A)^2 = -(1-z)\bar{s}, \quad (46c)$$

which are related via the equation

$$\bar{s} + \bar{t} + \bar{u} = 0. \quad (47)$$

The ITMD factorization was also investigated for other processes than dijets in proton-nucleus collisions. In [172] heavy quark pair production was studied and the problem of longitudinal gluons was discussed in depth. In [173] the effect of the genuine twists vs kinematic twists was studied in detail for dijets in DIS. Finally, neglecting the longitudinal gluon contribution, the ITMD framework was formulated and applied to the trijet production [155, 174].

3 ITMD with the Monte Carlo tool KATIE

KATIE [175] is a parton-level Monte Carlo event generator that can deal with space-like initial-state partons for arbitrary tree-level processes within the Standard Model. This means that it can be provided with k_T -dependent PDFs and that it will automatically calculate the necessary matrix elements with space-like initial-state partons to create parton-level event files. These event files can be chosen to be in the LHEF-format [176]. The k_T -dependent PDFs can be provided via TMDlib [177], or via independent grid files, which however must be in a specific format. Furthermore, KATIE can perform calculations within ITMD factorization, and automatically calculates the necessary gauge invariant matrix elements corresponding to the color structures associated with the several gluon distributions that appear in this factorization scheme. While KATIE primarily creates event files, it also provides tools to create histograms of differential distributions.

KATIE can be downloaded from <https://bitbucket.org/hameren/katie/downloads/>, and a description of use is provided in the manual there. Here, we provide some background on the Monte Carlo method it employs, elucidating the procedures to be followed when using KATIE.

In hybrid factorization like ITMD factorization, the cross section can be written as a $3n$ -dimensional integral

$$\sigma = \int d^{3n}\omega F(\omega), \quad (48)$$

where n is the number of final-state momenta. There are 4 initial-state variables, and $3n - 4$ final-state variables. For hadro-production of dijets at tree-level the number $n = 2$. The function F includes the collinear PDF, the TMDS, the flux factor, and the hard matrix elements. Given a probability density $G(\omega)$ in the integration space (or *phase space*) that is non-zero whenever $F(\omega)$ is non-zero, we can write

$$\sigma = \int d^{3n}\omega G(\omega) \frac{F(\omega)}{G(\omega)}. \quad (49)$$

The Monte Carlo method is based on the Central Limit Theorem, which dictates that if $\{\omega_1, \omega_2, \dots, \omega_N\}$ is a sequence of random phase space points, or *events*, independently drawn from density $G(\omega)$, then

$$\frac{1}{N} \sum_{i=1}^N \frac{F(\omega_i)}{G(\omega_i)} = \sigma + \mathcal{O}\left(\frac{1}{\sqrt{N}}\right). \quad (50)$$

Clearly, the approximation converges to the correct result faster if the fluctuation over the terms in the sum is smaller, with the optimum when $G(\omega) = F(\omega)/\sigma$. Successfully applying the Monte Carlo method means that one solves the problem of bringing $G(\omega)$ to this optimum to satisfactory degree. Reaching the optimum implies having solved the integration problem and eliminates the need for the Monte Carlo procedure. Satisfaction means that the result can be obtained within an

i	1	2
$\Phi_{gg^* \rightarrow gg}^{(i)}$	$\frac{1}{2N_c^2} (N_c^2 \mathcal{F}_{gg}^{(1)} - 2\mathcal{F}_{gg}^{(3)} + \mathcal{F}_{gg}^{(4)} + \mathcal{F}_{gg}^{(5)} + N_c^2 \mathcal{F}_{gg}^{(6)})$	$\frac{1}{N_c^2} (N_c^2 \mathcal{F}_{gg}^{(2)} - 2\mathcal{F}_{gg}^{(3)} + \mathcal{F}_{gg}^{(4)} + \mathcal{F}_{gg}^{(5)} + N_c^2 \mathcal{F}_{gg}^{(6)})$
$\Phi_{gg^* \rightarrow q\bar{q}}^{(i)}$	$\frac{1}{N_c^2 - 1} (N_c^2 \mathcal{F}_{gg}^{(1)} - \mathcal{F}_{gg}^{(3)})$	$-N_c^2 \mathcal{F}_{gg}^{(2)} + \mathcal{F}_{gg}^{(3)}$
$\Phi_{qg^* \rightarrow qg}^{(i)}$	$\mathcal{F}_{qg}^{(1)}$	$\frac{1}{N_c^2 - 1} (-\mathcal{F}_{qg}^{(1)} + N_c^2 \mathcal{F}_{qg}^{(2)})$

i	1	2
$K_{gg^* \rightarrow gg}^{(i)}$	$\frac{N_c}{C_F} \frac{(\bar{s}^4 + \bar{t}^4 + \bar{u}^4) (\bar{u}\hat{u} + \bar{t}\hat{t})}{\hat{t}\hat{u}\hat{s}\hat{s}}$	$\frac{N_c}{2C_F} \frac{(\bar{s}^4 + \bar{t}^4 + \bar{u}^4) (\bar{u}\hat{u} + \bar{t}\hat{t} - \bar{s}\hat{s})}{\hat{t}\hat{u}\hat{s}\hat{s}}$
$K_{gg^* \rightarrow q\bar{q}}^{(i)}$	$\frac{1}{2N_c} \frac{(\bar{t}^2 + \bar{u}^2) (\bar{u}\hat{u} + \bar{t}\hat{t})}{\bar{s}\hat{s}\hat{t}\hat{u}}$	$\frac{1}{4N_c^2 C_F} \frac{(\bar{t}^2 + \bar{u}^2) (\bar{u}\hat{u} + \bar{t}\hat{t} - \bar{s}\hat{s})}{\bar{s}\hat{s}\hat{t}\hat{u}}$
$K_{qg^* \rightarrow qg}^{(i)}$	$-\frac{\bar{u} (\bar{s}^2 + \bar{u}^2)}{2\hat{t}\hat{s}} \left(1 + \frac{\bar{s}\hat{s} - \bar{t}\hat{t}}{N_c^2 \bar{u}\hat{u}} \right)$	$-\frac{C_F}{N_c} \frac{\bar{s} (\bar{s}^2 + \bar{u}^2)}{\hat{t}\hat{u}}$

Table 2: The top table lists the combinations of the TMD gluon distributions listed in Table 1 that correspond to gauge invariant off-shell hard factors of the ITMD factorization formula. The bottom table gives explicit formulae for the LO off-shell gauge invariant hard factors of the ITMD factorization. The \hat{s} , \hat{t} and \hat{u} are ordinary Mandelstam variables, whereas \bar{s} , \bar{t} , \bar{u} are invariants where instead of the incoming off-shell gluon momentum its longitudinal component is used.

acceptable time, and in practice means finding a compromise between the number of terms needed, and the complexity of the algorithm to produce the sequence of events.

An advantage of the Monte Carlo method is that, given a “satisfactory” sequence *generator* to calculate the cross section σ , it can also be used to estimate differential distributions. Let $\varphi(\omega)$ be an observable, and $b_j(\varphi) = \theta(\varphi - \varphi_j)\theta(\varphi_{j+1} - \varphi)$ be a bin for this observable between values $[\varphi_j, \varphi_{j+1}]$, then

$$\frac{1}{N} \sum_{i=1}^N \frac{F(\omega_i)}{G(\omega_i)} b_j(\varphi(\omega_i)) = \int_{\varphi_j}^{\varphi_{j+1}} d\varphi \frac{d\sigma}{d\varphi} + \mathcal{O}\left(\frac{1}{\sqrt{N}}\right). \quad (51)$$

The idea of an *event file* is to store events ω_i and their *weight* $W_i = F(\omega_i)/G(\omega_i)$ to produce arbitrary distributions without having to redo the generation of events.

In the context of the foregoing, KATIE performs roughly speaking two tasks: it calculates the hard matrix elements, automatically and efficiently, as part of the evaluation of $F(\omega)$, and, provided with PDFs and TMDs, it creates reasonably-sized event files. In order to perform the first task, KATIE employs the Dyson-Schwinger approach to calculate tree-level helicity amplitudes numerically, as first proposed in [178] and also utilized in other tree-level programs, notably ALPGEN [179]. The feature of space-like initial-state momenta is dealt with following the auxiliary-parton method outlined in [145]. The second task is achieved through the application of many well-known optimization techniques, a few of which are worth to mention in order to understand the procedures in KATIE’s operation.

One is *adaptive importance sampling*, which optimizes adaptable probability densities iteratively, using the information of events generated so far in each iterative step. While being very effective, it can cause bias in those events, and they must not be used for the actual event file. Consequently, there must be a separate optimization stage before the generation of the event file starts. This happens for each partonic subprocess separately. Once this has been performed, the information of the optimized densities is stored, and is from then on used to generate an arbitrary number of event files.

Secondly, KATIE employs *rejection*. Phase space cuts are required to mimic detector acceptance and to avoid singularities in tree-level matrix elements. These typically are formulated in terms of variables that are non-trivial functions of the variables in ω that are actually generated, and cannot be implemented as exact integration bounds. Instead, the integrand $F(\omega)$ is imagined to vanish outside those phase space cuts, and a bigger enveloping space is generated. This leads to many events with $W_i = 0$, which are however not stored but are included in the eventual normalization of the weights. In order to achieve the unbiased normalization of the event weights in case several event files are generated, so called *raw* files are stored instead of actual event files, containing non-normalized weights and more statistical information. Event files in the LHF format can be extracted from these.

The third method that needs to be mentioned is *unweighting*. This is a statistical procedure to reduce the fluctuations of the weights W_i while keeping the event file sound. In practice this procedure “weeds out” low-weight events and reweighs remaining ones. The cross section estimate is not affected (is also not getting better) but it allows to reduce the required size of the event file. While it causes many events to get the same constant weight, there may occur events with higher weights.

The phase space is only $3n$ -dimensional, but it is much more convenient to write the events in terms of the $4n$ variables being the parton-level initial-state and final-state momenta. We will still denote events with the symbol ω . While all components of $F(\omega_i)$, like the matrix element, the PDFs, the strong coupling etc., can be re-evaluated using these, it is more convenient to also store their values besides W_i . This is useful if one wants to employ the *reweighting* procedure. For example, let an event file be created within hybrid k_T -factorization with a TMD $\mathcal{F}(\omega)$ (we simply imply that this function selects the appropriate variables from ω . Realize that this in practice includes the final-state ones due to the factorization scale dependence). Suppose a user has their own TMD \mathcal{F}' but only in a numerical form that cannot (yet) be married with KATIE or TMDlib. The value of $\mathcal{F}_i = \mathcal{F}(\omega_i)$ is stored for each event, and the event file can be transformed to be valid for \mathcal{F}' by multiplying

$$W_i \rightarrow W_i \frac{\mathcal{F}'(\omega_i)}{\mathcal{F}_i} \quad (52)$$

for each event. It will increase the fluctuation of the weights and reduce the quality of the event file, but most likely not in a drastic way.

As mentioned earlier, the use of KATIE is described in the manual, but below we present the complete single input card that allows to create event files for dijets within ITMD.

```
# Only QCD interaction, QED and Weak are on by default
switch = withQCD   Yes
switch = withQED   No
switch = withWeak  No
# List of processes
process = g g -> g g , factor = 1
process = g g -> u u~ , factor = Nf
process = u g -> g u , factor = 1
process = d g -> g d , factor = 1
process = s g -> g s , factor = 1
process = c g -> g c , factor = 1
process = b g -> g b , factor = 1
# In the process definition B A -> 1 2..., put initial state A off-shell
offshell = 0 1
itmdf = yes
# Collinear pdf set
lhaSet = CT10nlo
# Example directory and filenames below
tmdTableDir = /home/user/projects/TMDs/
tmdpdf = qg1 myGridFile-Fqg1.dat
tmdpdf = qg2 myGridFile-Fqg2.dat
tmdpdf = gg1 myGridFile-Fgg1.dat
tmdpdf = gg2 myGridFile-Fgg2.dat
tmdpdf = gg6 myGridFile-Fgg6.dat
Nflavors = 5
# Number of non-zero weight events to be spent on optimization
Noptim = 100,000
# Summing squared helicity amplitudes is more efficient in number of
# events (less fluctuation), but slower in time than sampling.
helicity = sum
# Center-of-mass (CM) energy, events will be in CM frame.
Ecm = 8160
# Jet definition, 1 and 2 refer to the final-state momenta
cut = {deltaR|1,2|} > 0.4
# {pT|1|} is the pT of final-state number 1
# {pT|1|1,2} is the hardest of the pTs of final-state number 1 and 2
cut = {pT|1|1,2} > 28
cut = {pT|1|1,2} < 35
cut = {pT|2|1,2} > 28
cut = {pT|2|1,2} < 35
# In the process definition B A -> 1 2...,
# initial-state A has equal-sign energy and z-component,
# while initial-state B has opposite-sign.
# The off-shell initial-state A has lower x than B,
# so the final state is boosted towards negative rapidity.
cut = {rapidity|1|} > -4.0
cut = {rapidity|2|} > -4.0
cut = {rapidity|1|} < -2.7
cut = {rapidity|2|} < -2.7
# Renormalization/factorization scale
scale = ({pT|1|}+{pT|2|})/2
```

4 Phenomenology of forward dijets

4.1 TMD gluon distributions

From the BK equation discussed in the earlier sections one can obtain TMD dipole gluon density. In this section we will use $k^2 = |\vec{k}_T|^2$ as argument of gluon density. This is the standard notation used in discussion of angular averaged distributions.

Let's define the following Fourier transforms [180, 181]

$$\mathcal{F}(x, k^2) = \frac{N_c}{\alpha_s(2\pi)^3} \int d^2b \int d^2r e^{ik \cdot r} \nabla_r^2 N(r, b, x), \quad \Phi(x, k^2) = \frac{1}{2\pi} \int d^2b \int \frac{d^2r}{r^2} e^{ik \cdot r} N(r, b, x) \quad (53)$$

as well as explicit relation between the two functions $\mathcal{F}(x, k^2)$ and $\Phi(x, k^2)$.

$$\mathcal{F}(x, k^2) = \frac{N_c}{4\alpha_s\pi^2} k^2 \nabla_k^2 \Phi(x, k^2), \quad \Phi(x, k^2) = \frac{\alpha_s\pi^2}{N_c} \int_{k^2}^{\infty} \frac{dl^2}{l^2} \ln \frac{l^2}{k^2} \mathcal{F}(x, l^2). \quad (54)$$

Since we are working in the large target approximation as well as in the forward limit *i.e.* we neglect any momentum transfer therefore we introduce the following normalization conditions for integration over the impact parameter

$$\int d^2\mathbf{b} S(b) = 1, \quad \int d^2\mathbf{b} S^2(b) = \frac{1}{\pi R^2} \quad (55)$$

where $S(b)$ is the profile function $S(b) = \theta(R - b)/\pi R^2$.

The momentum space equation for the $\Phi(x, k^2)$ assumes the form:

$$\Phi(x, k^2) = \Phi_0(x, k^2) + \bar{\alpha}_s \int_{x/x_0}^1 \frac{dz}{z} \int_0^{\infty} \frac{dl^2}{l^2} \left[\frac{l^2 \Phi(x/z, l^2) - k^2 \Phi(x/z, k^2)}{|k^2 - l^2|} + \frac{k^2 \Phi(x/z, k^2)}{\sqrt{(4l^4 + k^4)}} \right] - \frac{\bar{\alpha}_s}{\pi R^2} \int_{x/x_0}^1 \frac{dz}{z} \Phi^2(x/z, k^2). \quad (56)$$

where $\bar{\alpha} = N_c \alpha_s / \pi$.

The equation for $\mathcal{F}(x, k^2)$ is obtained from eq. (56) by inserting in the nonlinear part of it relation expressing $\Phi(x, k^2)$ in terms of $\mathcal{F}(x, k^2)$ and acting on the whole equation with the operator that transforms $\Phi(x, k^2)$ to $\mathcal{F}(x, k^2)$ see [181] for the details of this transformations. In the end one obtains [53, 181, 182]

$$\mathcal{F}(x, k^2) = \mathcal{F}_0(x, k^2) + \bar{\alpha}_s \int_{x/x_0}^1 \frac{dz}{z} \int_0^{\infty} \frac{dl^2}{l^2} \left[\frac{l^2 \mathcal{F}(x/z, l^2) - k^2 \mathcal{F}(x/z, k^2)}{|k^2 - l^2|} + \frac{k^2 \mathcal{F}(x/z, k^2)}{\sqrt{(4l^4 + k^4)}} \right] - \frac{2\alpha_s^2\pi}{N_c R^2} \int_{x/x_0}^1 \frac{dz}{z} \left[\left[\int_{k^2}^{\infty} \frac{dl^2}{l^2} \mathcal{F}(x/z, l^2) \right]^2 + \mathcal{F}(x/z, k^2) \int_{k^2}^{\infty} \frac{dl^2}{l^2} \ln \left(\frac{l^2}{k^2} \right) \mathcal{F}(x/z, l^2) \right]. \quad (57)$$

The linear part of the equation above is the well known BFKL kernel while the nonlinear part is the triple pomeron vertex. The triple pomeron vertex has such property that it is dominated by the anticollinear pole. We see that as one evaluates the gluon at lower and lower values of k^2 the integration in the nonlinear term is over larger domain giving larger contribution and suppressing the gluon density. One can also see that in the collinear limit the nonlinear term completely drops and one is left with linear equation.

$$\mathcal{F}(x, k^2) = \mathcal{F}^{(0)}(x, k^2) + \bar{\alpha}_s \int_{x/x_0}^1 \frac{dz}{z} \int_{k_0^2}^{k^2} dk'^2 \frac{\mathcal{F}(x/z, k'^2)}{k^2}. \quad (58)$$

4.2 BK equation within Kwiecinski Martin Staśto model

The (57) is a leading order BK equation for dipole gluon density. In order to make it applicable to phenomenology it has been extended to account for higher order corrections following Kwiecinski-Martin-Stasto (KMS) prescription [183] that was originally applied to the BFKL equation. Those include

- kinematical constraints which enforce that the virtuality of exchanged gluon is dominated by its transverse component $k^2 = |\vec{k}_T|^2$. This constrain suppresses anticollinear pole and therefore suppresses the diffusion into infrared
- nonsingular at small z pieces of the splitting function
- running coupling constant
- sea quark singlet contribution to match the DGLAP limit at large z

With these corrections the equation assumes the form [181]

$$\begin{aligned}
\mathcal{F}(x, k^2) = & \mathcal{F}_0(x, k^2) \\
& + \frac{\alpha_s(k^2)N_c}{\pi} \int_{x/x_0}^1 \frac{dz}{z} \int_{k_0^2}^{\infty} \frac{dl^2}{l^2} \left\{ \frac{l^2 \mathcal{F}\left(\frac{x}{z}, l^2\right) \theta\left(\frac{k^2}{z} - l^2\right) - k^2 \mathcal{F}\left(\frac{x}{z}, k^2\right)}{|l^2 - k^2|} + \frac{k^2 \mathcal{F}\left(\frac{x}{z}, k^2\right)}{\sqrt{4l^4 + k^4}} \right\} \\
& + \frac{\alpha_s(k^2)}{2\pi k^2} \int_{x/x_0}^1 dz \left\{ \left(P_{gg}(z) - \frac{2N_c}{z} \right) \int_{k_0^2}^{k^2} dl^2 \mathcal{F}\left(\frac{x}{z}, l^2\right) + z P_{gq}(z) \Sigma\left(\frac{x}{z}, k^2\right) \right\} \\
& - \frac{2\pi\alpha_s^2(k^2)}{N_c R^2} \left\{ \left[\int_{k^2}^{\infty} \frac{dl^2}{l^2} \mathcal{F}(x, l^2) \right]^2 + \mathcal{F}(x, k^2) \int_{k^2}^{\infty} \frac{dl^2}{l^2} \ln\left(\frac{l^2}{k^2}\right) \mathcal{F}(x, l^2) \right\}, \quad (59)
\end{aligned}$$

where $\Sigma(x, k^2)$ is a sea quark distribution obeying essentially DGLAP equation in unintegrated form (further details can be found in [181]). Please note that in the equation above lower cut in $k^2 = k_0^2$ was introduced. The origin of the cut is related to the method of solving of the equation and in principle can be set to arbitrarily small value.

In Ref. [12], the following initial condition for Eq. (59) was fitted to the F_2 proton structure data from HERA [184]

$$\mathcal{F}_0(x, k^2) = \frac{\alpha_s(k^2)}{2\pi k^2} \int_x^1 dz P_{gg}(z) \frac{x}{z} g\left(\frac{x}{z}, k_0^2\right), \quad (60)$$

with

$$xg(x) = N(1-x)^\beta(1-xD). \quad (61)$$

For $k^2 \leq 1 \text{ GeV}^2$, the gluon distribution was taken as $\mathcal{F}(x, k^2) = k^2 \mathcal{F}(x, 1)$, which is motivated by the shape obtained from the solution of the LO BK equation in the saturation regime [185].

The fitting procedure gave the following numerical values for the parameters: $N = 0.94$, $\beta = 18.6$, $D = -82.1$ and $R = 2.40 \text{ GeV}^{-1}$. The overall quality of the fit was good, with $\chi^2/\text{ndof} = 1.73$. We shall refer to this gluon distribution as the Kutak-Sapeta or KS gluon.

For completeness, the fit of linearized version of Eq. (59), *i.e.* with the last term dropped, was performed as well, and the following parameters were obtained: $N = 0.004$, $\beta = 26.7$, $D = -51102$ and $\chi^2/\text{ndof} = 3.86$. The presence of the parameter R , characterizing the target, allows one to obtain dipole gluon distribution of nuclei. In order to do that, one uses relation $R_A = d A^{1/3} R$, which in the end gives the enhancement by $A^{1/3}$ of the nonlinear term for gluon density normalized to the number of nucleons [12]. The parameter d is a phenomenological factor that was varied between $d = 0.5$ and $d = 1.0$. In the following computations we used the ‘‘least saturation’’ scenario with $d = 0.5$.

4.3 The Sudakov Resummation

An important class of perturbative corrections to scattering process, appearing when the emitted partons are both collinear and soft, is resummed in terms of the Sudakov form factor [186–188]. It appears due to not exact cancellation of virtual corrections and real corrections, as a consequence of certain exclusivity of the final state. In the processes considered here the largest effect of the Sudakov is expected to affect the cross section when the jets are in nearly back-to-back configuration. The large logarithm comes since the transverse momenta of jets can be sizable while the imbalance

k_T of incoming space-like parton is small. The effect of Sudakov form factor is to suppress the back-to-back configuration and enhance the moderate angle part of the distribution, leading to so-called broadening. Within the small- x formalism the Sudakov form factor can be factorized, in the coordinate space, from the hard process [186–188]. The complete cross-section accounting for the Sudakov form factor reads:

$$\frac{d\sigma^{\text{pA} \rightarrow j_1 j_2 + X}}{d^2 P_T d^2 k_T dy_1 dy_2} = \sum_{a,c,d} x_p \sum_{i=1}^2 \mathcal{K}_{ag^* \rightarrow cd}^{(i)}(P_T, k_T; \mu) \times \int db_T b_T J_0(b_T k_T) f_{a/p}(x_p, \mu_b) \tilde{\Phi}_{ag \rightarrow cd}^{(i)}(x_A, b_T) e^{-S^{ag \rightarrow cd}(\mu, b_T)}, \quad (62)$$

where $\tilde{\Phi}_{ag \rightarrow cd}^{(i)}$ is the Fourier transform of the TMD gluon distributions and $S^{ag \rightarrow cd}$ are the Sudakov factors written for each channel

$$S^{ab \rightarrow cd}(\mu, b_T) = \sum_{i=a,b,c,d} S_p^i(\mu, b_T) + \sum_{i=a,c,d} S_{np}^i(\mu, b_T), \quad (63)$$

where S_p^i and S_{np}^i are the perturbative and non-perturbative contributions. The perturbative Sudakov factors, including double and single logarithms, are given by [186, 189]

$$S_p^{qg \rightarrow qg}(\mu, b_T) = \int_{\mu_b^2}^{\mu^2} \frac{dq_T^2}{q_T^2} \left[2(C_F + C_A) \frac{\alpha_s}{2\pi} \ln \left(\frac{\mu^2}{q_T^2} \right) - \left(\frac{3}{2} C_F + C_A \beta_0 \right) \frac{\alpha_s}{\pi} \right], \quad (64)$$

$$S_p^{gg \rightarrow gg}(\mu, b_T) = \int_{\mu_b^2}^{\mu^2} \frac{dq_T^2}{q_T^2} \left[4C_A \frac{\alpha_s}{2\pi} \ln \left(\frac{\mu^2}{q_T^2} \right) - 3C_A \beta_0 \frac{\alpha_s}{\pi} \right], \quad (65)$$

where $\beta_0 = (11 - 2n_f/N_c)/12$. The $gg \rightarrow q\bar{q}$ channel is negligible in kinematic domain considered here. In the above the scale μ_b is the inverse of the impact parameter:

$$\mu_b = 2e^{-\gamma_E}/b_* \quad (66)$$

with

$$b_* = b_T / \sqrt{1 + b_T^2/b_{\text{max}}^2}. \quad (67)$$

Given this selection, the scale μ_b becomes constant at the point of high b_T , where its value is determined to be $2e^{-\gamma_E}/b_{\text{max}}$, which is considerably greater than Λ_{QCD} . Following Ref. [190], we will adopt $b_{\text{max}} = 0.5, \text{GeV}^{-1}$.

For completeness we comment briefly on DGLAP based prescriptions for incorporating the Sudakov form factor. The method relies on constructing the Sudakov form factor from DGLAP splitting function and using it to reshuffle events according to relation between hard scale and transverse momentum of the gluon. In such constructions one chooses some inclusive quantity to be unmodified while allowing for modification of unintegrated quantity. Two such methods were presented in [24, 191]. In the former the total cross section was preserved while in the later the integrated gluon density was unmodified.

4.4 Kutak-Sapeta (KS) gluon distribution

We shall now discuss the KS gluon, introduced above, in variants with and without the Sudakov resummation. The parameters were fixed by the original fit [12] with no Sudakov factors and the gluon was later used without any modifications. Hence, combining it with the Sudakov does not introduce new parameters. This is true because the perturbative part (64) and (65) is parameter-free while the non-perturbative terms are universal in the kinematic domain of our study [192].

We introduce the Sudakov effects into the KS gluon distribution following the formalism described above. In addition, for reference, we use two methods employed in our earlier studies [24, 191]. Those calculations used the Sudakov form factor, understood as the DGLAP evolution

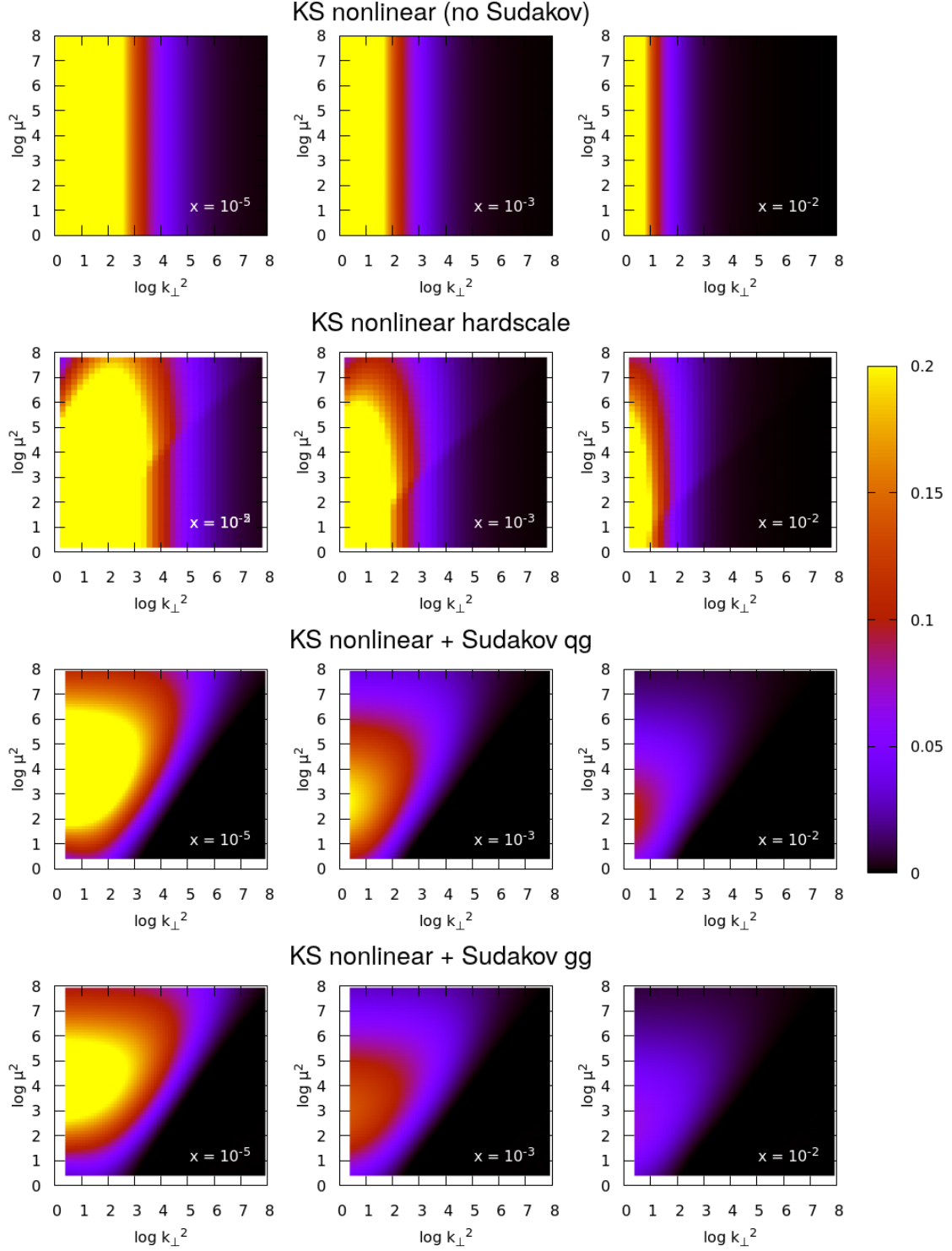


Figure 7: KS gluon distribution, without and with the Sudakov form factors. The second row corresponds to the simple model-Sudakov given in Eq. (68), while the third and the fourth rows show results obtained with the Sudakov factors derived from QCD and given in Eqs. (63)–(65).

kernel, that has been applied on the top of the gluon TMD, together with constrains such as unitarity. Those methods should therefore be considered as models, in contrast to the proper resummation of Sudakov logarithms described in the preceding section. Nevertheless, the approaches used in Refs. [24, 191] were phenomenologically successful (see also [14]), and it is therefore useful and interesting to compare the predictions of those simplistic models with the proper way of including the Sudakov effects into the small- x gluon.

The reference models are:

- Model 1: The survival probability model [191], where the Sudakov factor of the form [193]

$$T_s(\mu_F^2, k_T^2) = \exp \left(- \int_{k_T^2}^{\mu_F^2} \frac{dk_T'^2}{k_T'^2} \frac{\alpha_s(k_T'^2)}{2\pi} \sum_{a'} \int_0^{1-\Delta} dz' P_{a'a}(z') \right), \quad (68)$$

is imposed at the level of the cross section. This procedure corresponds to performing a DGLAP-type evolution from the scale $\mu_0 \sim k_T$ to μ , decoupled from the small- x evolution.

- Model 2: The model with a hard scale introduced in Ref. [24]. The Sudakov form factor of the same form as in Eq. (68) is imposed on top of the KS gluon distribution in such a way that, after integration of the resulting hard scale dependent gluon TMD, one obtains the same result as by integrating the KS gluon distribution.

In Fig. 7, we show the KS gluon distributions, with and without Sudakov form factors, as functions of the transverse momentum k_T and the hard scale μ . Three columns correspond to three different x values. The first row shows the original KS gluon distribution, which, as expected, does not depend on the value of μ . In the second row, we show the KS hardscale gluon distribution of Ref. [24] (the other model [191] does not allow one to plot gluon distribution, as it applies Sudakov effects at the cross section level via a reweighting procedure). Here, the dependence on μ is non-trivial and we see that the gluon develops a maximum in that variable. As shown in the figure, this maximum is rather broad. In the third and the fourth row of Fig. 7, we present the KS gluon distribution with the Sudakov form factor from Eqs. (63)–(65). As explained earlier, this gluon exists in two versions, one for the qg and the other for the gg channel. The dependence on k_T and μ is qualitatively similar between these gluons and the naive KS hardscale gluon distribution. In the former case, however, the peak is significantly narrower in μ as compared to the naive model of Ref. [24]. It is interesting to note that the qg gluon is broader than the gg gluon. This can be understood by comparing the colour factors in the Sudakov functions (64) and (65). Since the colour factor for the gg channel is larger than for the qg , the Sudakov suppression is stronger along the μ direction in the former case.

We have as well computed linear versions of the KS gluon distributions with the Sudakov, using the KS linear gluon distribution of Ref. [12]. The gluons discussed in this section are available publicly as part of the `KS` package and can be downloaded from <http://nz42.ifj.edu.pl/~sapeta/KSgluon-2.0.tar.gz>.

4.5 ITMD gluons distributions

In the limit of small x and large number of colors (Gaussian approximation), the gluons listed in the table (1) can be expressed in terms of dipole gluon density as [157]

$$\mathcal{F}_{qg}^{(1)}(x, |\vec{k}_T|) = xG^{(2)}(x, |\vec{q}_T|), \quad (69)$$

$$\mathcal{F}_{qg}^{(2)}(x, |\vec{k}_T|) = \int d^2q_T xG^{(1)}(x, |\vec{q}_T|) F(x, |\vec{k}_T - \vec{q}_T|), \quad (70)$$

$$\mathcal{F}_{gg}^{(1)}(x, |\vec{k}_T|) = \int d^2q_T xG^{(2)}(x, |\vec{q}_T|) F(x, |\vec{k}_T - \vec{q}_T|), \quad (71)$$

$$\mathcal{F}_{gg}^{(2)}(x, |\vec{k}_T|) = - \int d^2q_T \frac{(\vec{k}_T - \vec{q}_T) \cdot \vec{q}_T}{|\vec{q}_T|^2} xG^{(2)}(x, |\vec{q}_T|) F(x, |\vec{k}_T - \vec{q}_T|), \quad (72)$$

$$\mathcal{F}_{gg}^{(6)}(x, |\vec{k}_T|) = \int d^2q_T d^2q_T' xG^{(1)}(x, |\vec{q}_T|) F(x, |\vec{q}_T'|) F(x, |\vec{k}_T - \vec{q}_T - \vec{q}_T'|). \quad (73)$$

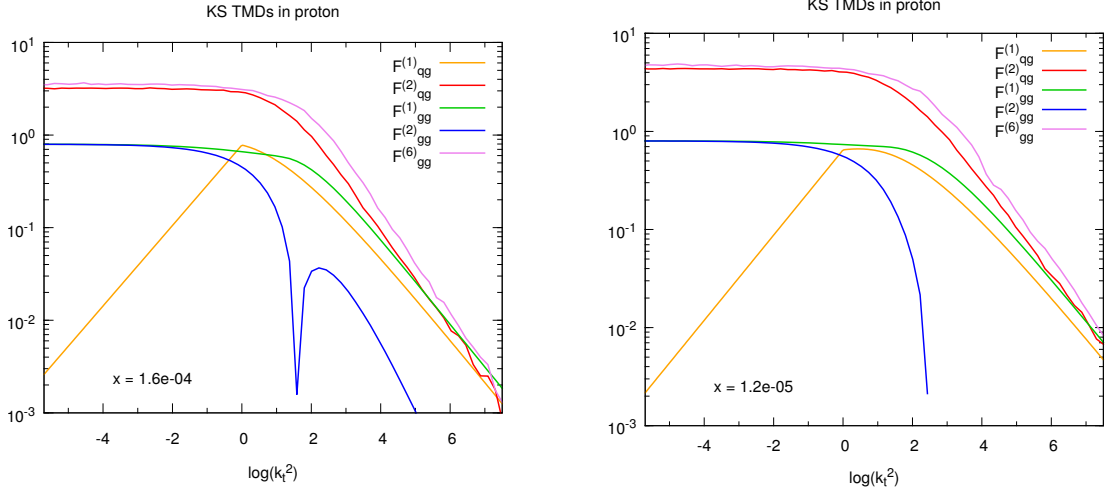


Figure 8: The KS gluon TMDs as a function of $\log(|\vec{k}_T|^2/\text{GeV}^2)$ at $x = 1.6 \cdot 10^{-4}$ for the proton (left) and the lead nucleus (right). Since $\mathcal{F}_{gg}^{(2)}$ goes negative, its absolute value is shown on the figures.

where

$$xG^{(2)}(x, |\vec{k}_T|) = \frac{N_c |\vec{k}_T|^2 S_\perp}{2\pi^2 \alpha_s} F(x, |\vec{k}_T|) , \quad (74)$$

and $F(x, |\vec{k}_T|)$ is a Fourier transform of the fundamental dipole

$$F(x, |\vec{k}_T|) = \int \frac{d^2\vec{r}}{(2\pi)^2} e^{-i\vec{k}_T \cdot \vec{r}} \langle \text{Tr} [U(\vec{r})U^\dagger(0)] \rangle_x / N_c, \quad (75)$$

The gluons listed above form a set from which one can construct the gluon densities $\Phi^{(i)}$ entering the ITMD factorization formula (42) as obtained in [30]:

$$\Phi_{qg \rightarrow qg}^{(1)} = \mathcal{F}_{qg}^{(1)} \quad , \quad \Phi_{qg \rightarrow qg}^{(2)} \approx \mathcal{F}_{qg}^{(2)} \quad (76)$$

$$\Phi_{gg \rightarrow q\bar{q}}^{(1)} \approx \mathcal{F}_{gg}^{(1)} \quad , \quad \Phi_{gg \rightarrow q\bar{q}}^{(2)} \approx -N_c^2 \mathcal{F}_{gg}^{(2)} \quad (77)$$

$$\Phi_{gg \rightarrow gg}^{(1)} \approx \frac{1}{2} \left(\mathcal{F}_{gg}^{(1)} + \mathcal{F}_{gg}^{(6)} \right) \quad , \quad \Phi_{gg \rightarrow gg}^{(2)} \approx \mathcal{F}_{gg}^{(2)} + \mathcal{F}_{gg}^{(6)} . \quad (78)$$

4.6 ITMD distributions from KS gluon

All the gluon TMDs (69)-(73) can be calculated from a single $xG^{(2)}(x, |\vec{k}_T|)$ distribution in the above Gaussian approximation. However, because the KS gluon provides directly an impact-parameter-integrated distribution, it is not straightforward to identify S_\perp and obtain $F(x, |\vec{k}_T|)$ from Eq. (74). To address this issue, we applied the following procedure [194]. We first computed the dipole cross section $\sigma_{\text{dipole}}(x, r = |\mathbf{r}|) = 2 \int d^2b N_F(x, \mathbf{r})$ from $xG^{(2)}(x, |\vec{k}_T|)$ by inverse Fourier transformation of Eq. (75), and then defined S_\perp as its value at large r , *i.e.* when it saturates (since in that limit $N_F \rightarrow 1$):

$$\frac{1}{2} \sigma_{\text{dipole}}(x, r = \infty) = S_\perp(x) = \lim_{r \rightarrow \infty} \frac{4\pi^3}{N_c} \alpha_s \int \frac{d|\vec{k}_T|}{|\vec{k}_T|} \left[1 - J_0(r|\vec{k}_T|) \right] xG^{(2)}(x, |\vec{k}_T|) . \quad (79)$$

We can now obtain $F(x, |\vec{k}_T|)$ and calculate all the needed gluon TMDs. Their behavior as a function of $k_t = |\vec{k}_T|$ is plotted in Fig. 8, both for the proton and the lead nucleus. The small

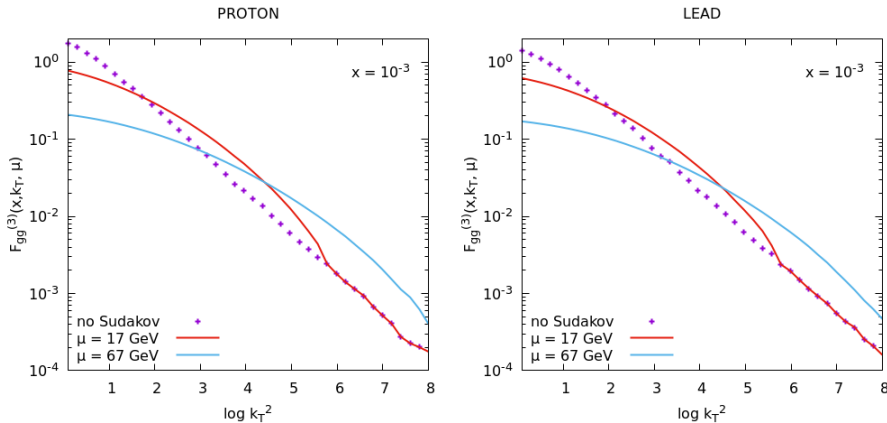


Figure 9: The WW gluon density in the proton (left) and lead (right), with and without Sudakov resummation, as a function of the transverse momentum of the gluon, for various values of the hard scale.

mismatch between their high- k_t behavior, expected due to the initial condition for the x evolution, can be observed.

Similarly, we computed [195] the ITMD distributions from the KS gluon with the proper QCD Sudakov, shown in Fig. 7.

Within the Gaussian approximation, one can also derive the following formula for the WW gluon density [194]

$$\mathcal{F}_{gg}^{(3)}(x, |\vec{k}_T|) = \frac{2\pi^2 \alpha_s}{N_c |\vec{k}_T|^2 S_\perp} \frac{1}{2} \int_{|\vec{k}_T|^2} d^2 k'_T \ln \frac{|\vec{k}'_T|^2}{|\vec{k}_T|^2} \int \frac{d^2 q_T}{|\vec{q}_T|^2} \mathcal{F}_{gg}^{(1)}(x, |\vec{q}_T|) \mathcal{F}_{gg}^{(1)}(x, |\vec{k}'_T - \vec{q}_T|), \quad (80)$$

where $\mathcal{F}_{gg}^{(1)}$ is the dipole gluon density and S_\perp is the target's transverse area.

Using the procedure described above, we computed also the WW gluon, which we show in Fig. 9 in proton (left) and lead (right), with and without Sudakov form factors, as functions of the transverse momentum $|\vec{k}_T|$ and the hard scale μ , for one particular $x = 10^{-3}$. (The gluon density is available from the TMDlib [177].)

First of all, let us notice that the WW gluon distribution has no maximum, contrary to the dipole gluon [12, 194]. Secondly, we see that the Sudakov factor suppresses the gluon distribution at low $|\vec{k}_T|$ and enhances it at higher $|\vec{k}_T|$. Because the Sudakov form factor is derived in the regime $\mu \propto |\vec{p}_T| \gg |\vec{k}_T|$, we apply it only to that part of the gluon density where $\mu > |\vec{k}_T|$. In the remaining domain, we use the gluon without Sudakov, given in Eq. (80). This is visible in Fig. 9 as a kink of the curve corresponding to $\mu = 17$ GeV. (A similar kink exists also for the $\mu = 67$ GeV curve but it is located at larger values of $\log |\vec{k}_T|^2$.)

All the ITMD gluons discussed in this above are available publicly and can be downloaded from <http://nz42.ifj.edu.pl/~sapeta/itmd-KS.tar.gz>.

4.7 Forward dijets at the LHC

In the following section we review some existing predictions for forward dijet production in proton-proton and proton-lead collisions at LHC energies, obtained within the ITMD framework. We also include some new computations, not published before.

Before we proceed, it is important to mention, that the first predictions for forward dijets in saturation formalism using the ITMD, that – as discussed in Section 2.3 – approximates the CGC for sufficiently large transverse momenta, appeared in [194]. This computation significantly improved the predictions of [23] obtained with k_T -factorization, which is not entirely accurate at small dijet imbalance. Later, in [196] a full computation within CGC was compared to ITMD, confirming, that at larger transverse momenta ITMD is adequate.

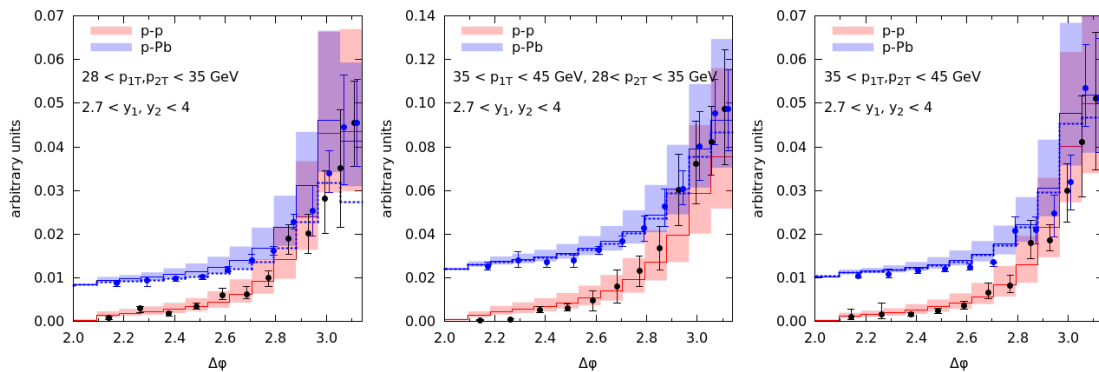


Figure 10: Broadening of azimuthal correlations in p-Pb collisions vs p-p collisions for different sets of cuts imposed on the jets’ transverse momenta. The blue and red bands show the normalized differential cross sections in azimuthal angle $\Delta\phi$, respectively for p-Pb and p-p, shifted so that they match in the first bin. The points show the experimental data [25] for p-p and p-Pb, where the p-Pb data were shifted by a pedestal, so that the values in the bin $\Delta\phi \sim \pi$ are the same. Theoretical calculations are represented by the histograms with uncertainty bands coming from varying the scale by factors 1/2 and 2.

None of the above computations included the Sudakov resummation, however. In [14] a calculation has been performed that included both the full ITMD and the Sudakov resummation “model” [191], based on the reweighting the events with the DGLAP Sudakov form factor. The Authors compared the shape of the obtained azimuthal dijet correlations for proton-proton and proton-lead with those obtained by ATLAS collaboration [25] (no dijet cross section was actually measured, only the conditional yields). Interestingly, when the shapes of the azimuthal correlations for p-p and p-Pb are stacked together so that they match in the first bin, one can clearly see broadening of the p-Pb cross section. It turns out, that similar broadening is obtained within the ITMD, if both the saturation as well as the Sudakov resummation are present. We show this result in Fig. 10.

In the following, we shall report on further advances in dijet computations within ITMD, with the full Sudakov resummation [197]. In particular, we will present the numerical results for the differential cross sections in terms of the azimuthal angle $\Delta\phi$ between the leading and the sub-leading jets for the proton-proton and the proton-lead collisions at LHC energies. We shall also discuss the nuclear modification ratio R_{p-Pb}

$$R_{p-Pb} = \frac{d\sigma^{p+Pb}}{A \frac{d\sigma^{p+p}}{d\mathcal{O}}}, \quad (81)$$

where \mathcal{O} is a differential related to an observable. Finally, we shall investigate differential cross sections in the rapidity of the leading and sub-leading jet.

The cross sections were computed using the KATIE Monte Carlo program [175] within the ITMD factorization, both described in the preceding Sections. We considered the proton-proton and proton-lead collisions at $\sqrt{s} = 5.02$ TeV, 8.16 TeV and 8.8 TeV per nucleon. For proton-proton collisions, we also computed the proton-proton cross section for $\sqrt{s} = 14$ TeV. In order to define the leading and the sub-leading jets, mentioned above, we used the anti- k_T jet clustering algorithm [198] with a radius of $R = 0.4$. Since our computation is leading order, the jet algorithm is actually equivalent to a simple cut in rapidity-azimuthal plane. Motivated by the current and planned LHC experiments, we applied the following cuts to the transverse momentum of these jets:

- i)* $28 \text{ GeV} < p_{T1}, p_{T2} < 35 \text{ GeV}$,
- ii)* $35 \text{ GeV} < p_{T1}, p_{T2} < 45 \text{ GeV}$,
- iii)* $35 \text{ GeV} < p_{T1} < 45 \text{ GeV}$ and $28 \text{ GeV} < p_{T2} < 35 \text{ GeV}$,
- iv)* $p_{T1}, p_{T2} > 10 \text{ GeV}$,

v) $p_{T1}, p_{T2} > 20$ GeV.

Specifically, we used the first three cuts *i) – iii)* for the transverse momentum of the jets in the rapidity range $2.7 < y_1^*, y_2^* < 4.0$, both for proton-proton and proton-lead collisions at $\sqrt{s} = 8.16$ TeV. These cuts correspond to the FCal calorimeter of the ATLAS detector and are motivated by the measurement [25]. The last two cuts *iv) – v)* were applied in the rapidity range $3.8 < y_1^*, y_2^* < 5.1$, both for proton-proton and proton-lead collisions at $\sqrt{s} = 5.02$ TeV, and 8.8 TeV energies per nucleon. These correspond to the planned FoCal extension of the ALICE detector [27]. For the same kinematic domain (rapidity and transverse momentum cuts for the jets), we also considered protons collisions at $\sqrt{s} = 14$ TeV (proton-lead collisions are not feasible at this energy). The result for 5.02 TeV and 14 TeV were not published in [197] and are thus new.

The factorization and renormalization scales were set using the transverse momentum of the leading and the sub-leading jets $\mu = (p_{T1} + p_{T2})/2$. For the TMD gluon distributions, we used the ones calculated in [194] based on the Kutak-Sapeta (KS) fit of the dipole gluon density [12], as described in the preceding subsections. For the collinear PDFs we used the CTEQ10NLO PDF set [199] from LHAPDF6 [200]. For the computation of the cross sections, we included the channels $gg^* \rightarrow qg$, with five quark flavours, and $gg^* \rightarrow gg$. The channel $gg^* \rightarrow \bar{q}q$ was neglected because its contribution, for the considered kinematic domain, is quite small [12, 194].

Let us now discuss the results. In Fig. 11 we show the results for the azimuthal correlations for p-p and p-Pb collisions in the ATLAS kinematics at $\sqrt{s} = 8.16$ TeV. We compare the Sudakov resummation obtained via two methods, the full- b space resummation (dotted) and the simplified approach, where the collinear PDF is not affected by the Sudakov form factor. As can be seen, they differ a bit, but as we shall see below, the difference cancels in the nuclear modification ratio, thus does not affect the saturation signal. Moreover, as we also show below, there are very large scale uncertainties, within which both methods are qualitatively similar. In our computations we used the ITMD factorization alone, without parton shower or hadronisation corrections. In order to asses this effect, we computed cross section with PYTHIA [201, 202] with all correction turned on, and then just with initial-state parton shower. The latter roughly corresponds to the TMD framework (as discussed eg. in [203]), therefore both calculations allow for extraction of a “correction factor”. We repeated the same procedure using the nuclear PDFs in PYTHIA. In Fig. 12 we applied that correction to KATIE results and compared with PYTHIA computations. Although the correction factor is rather large, as we shall see below it does not affect the saturation signal in the nuclear modification ratio. Next, in Fig. 13 we show the error bands due to both scale variation. Finally, in Fig. 14 we compute the nuclear modification ratio. For all three p_T cuts, we show the ITMD result with simplified Sudakov resummation, with the full- b space resummation, and the result where the non-perturbative correction factor from PYTHIA was applied. We also compute the error band due to scale variation and due to the correction factor. We see, that the saturation effect due to the nonlinear evolution is visible, but not very significant for the considered kinematics. For the lower p_T cut we observe suppression of about 15%, but the uncertainty due to the correction factor is not much less. Interestingly (but understandably) this error decreases for larger p_T bins.

Next, we move on to the more forward region with FoCal kinematics. Here we focus first on the $p_T > 10$ GeV cut. The results for azimuthal correlations are shown in Fig. 15. In one figure we show ITMD result with Sudakov obtained via both models, as well as PYTHIA corrections and errorbands, as discussed before. In Fig. 16 we compute the nuclear modification ration for that case. As can be seen from the plot, the suppression due to saturation is very large, about 25-30%, and is not destroyed by the errors, both due to the scale variation and due to the non-perturbative effects. In Fig. 17 we show latest results, where we compare p-p and p-Pb cross sections at different energies, computed also with larger $p_T > 20$ GeV cut. As expected, the difference between p-p and p-Pb is smaller in that case. Next, in Fig. 18-19 we present latest results for rapidity distributions for the two p_T cuts, for the leading jet, and the sub-leading jet. As the shape of the rapidity distribution is correlated with the x dependence, and thus with the evolution in the energy, measurement of the rapidity distribution may provide a valuable discriminatory tool for the evolution equations. Finally, in Fig. 20 we show the nuclear modification ratio for the two energies and both p_T cuts. As can be seen, with forward FoCal kinematic, even with the p_T cut of 20 GeV the suppression is about 20%.

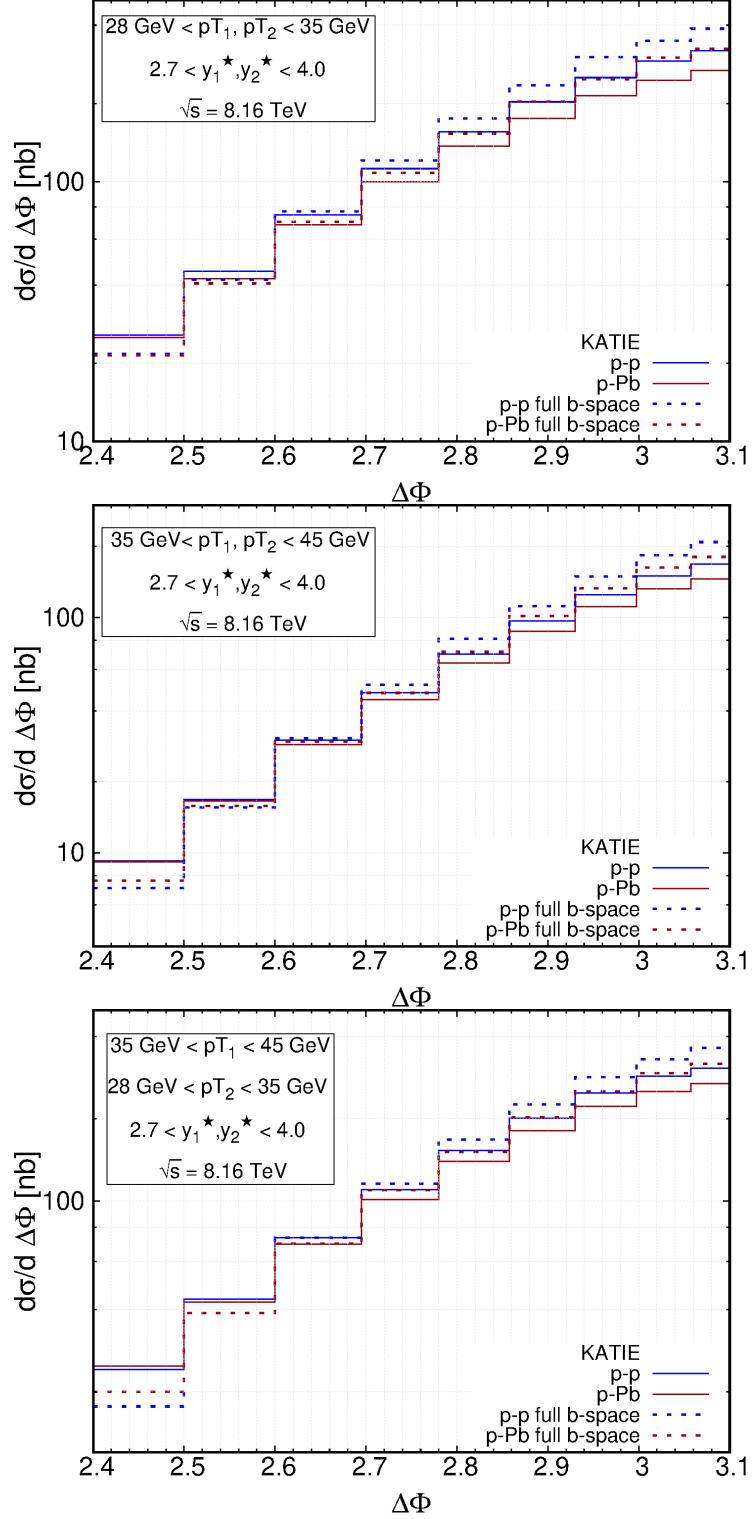


Figure 11: The differential cross sections in terms of the azimuthal angle $\Delta\phi$ between the leading and the sub-leading jets for the proton-proton and the proton-lead collisions at $\sqrt{s} = 8.16$ TeV in the FCal ATLAS kinematics. These were computed using KATIE within the ITMD factorization formula with: the simplified Sudakov resummation Eq. (42) (solid lines), the full b -space resummation Eq. (62) (dotted lines). The plots were taken from [197].

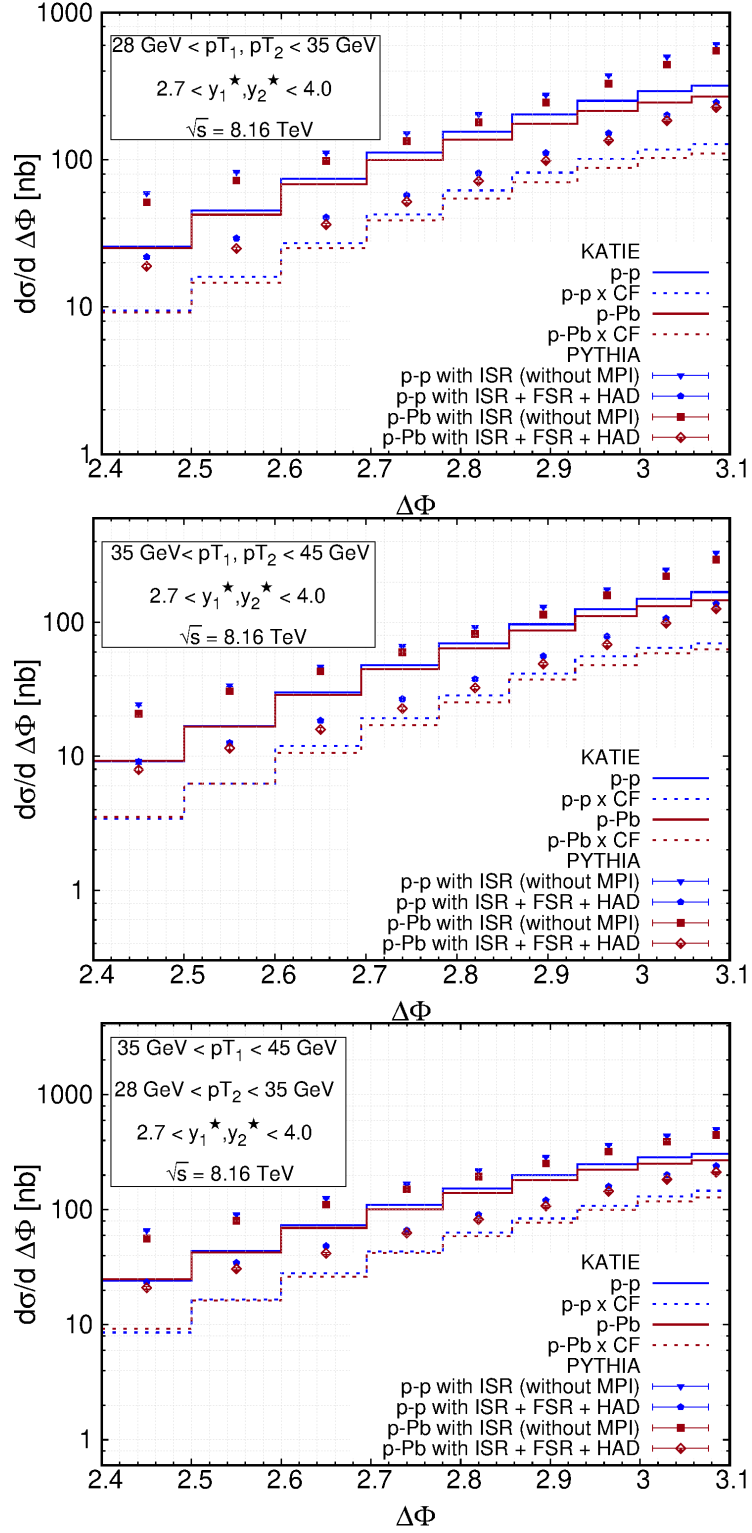


Figure 12: The differential cross sections in terms of the azimuthal angle $\Delta\phi$ between the leading and the sub-leading jets for the proton-proton and the proton-lead collisions at $\sqrt{s} = 8.16$ TeV in the FCal ATLAS kinematics. The solid lines represent the results from KATIE computed within the ITMD approach, the points represent the results from PYTHIA with different components, and the dotted lines represent the KATIE results corrected with the non-perturbative correction factor extracted from PYTHIA. The plots were taken from [197].

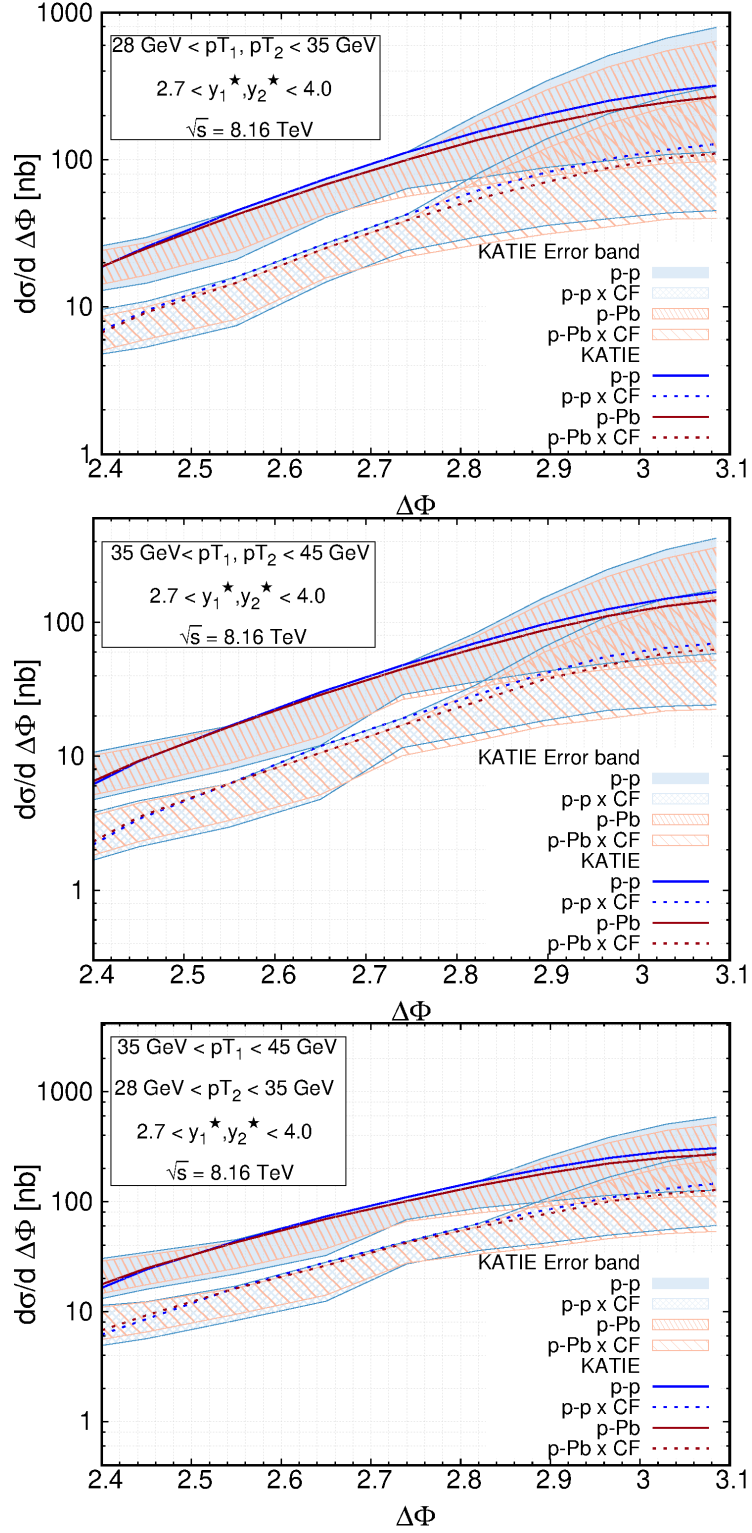


Figure 13: The differential cross sections in terms of the azimuthal angle $\Delta\phi$ between the leading and the sub-leading jets for the proton-proton and the proton-lead collisions at $\sqrt{s} = 8.16 \text{ TeV}$ in the FCal ATLAS kinematics. The solid lines represent the results from KATIE computed within the ITMD approach, and the dotted lines represent the KATIE results corrected with the non-perturbative correction factor extracted from PYTHIA. The bands represent the error due to the variation of the factorization/renormalization scales from a value of $(p_{T1} + p_{T2})/2$ by a factor of 1/2 and 2. The plots were taken from [197].

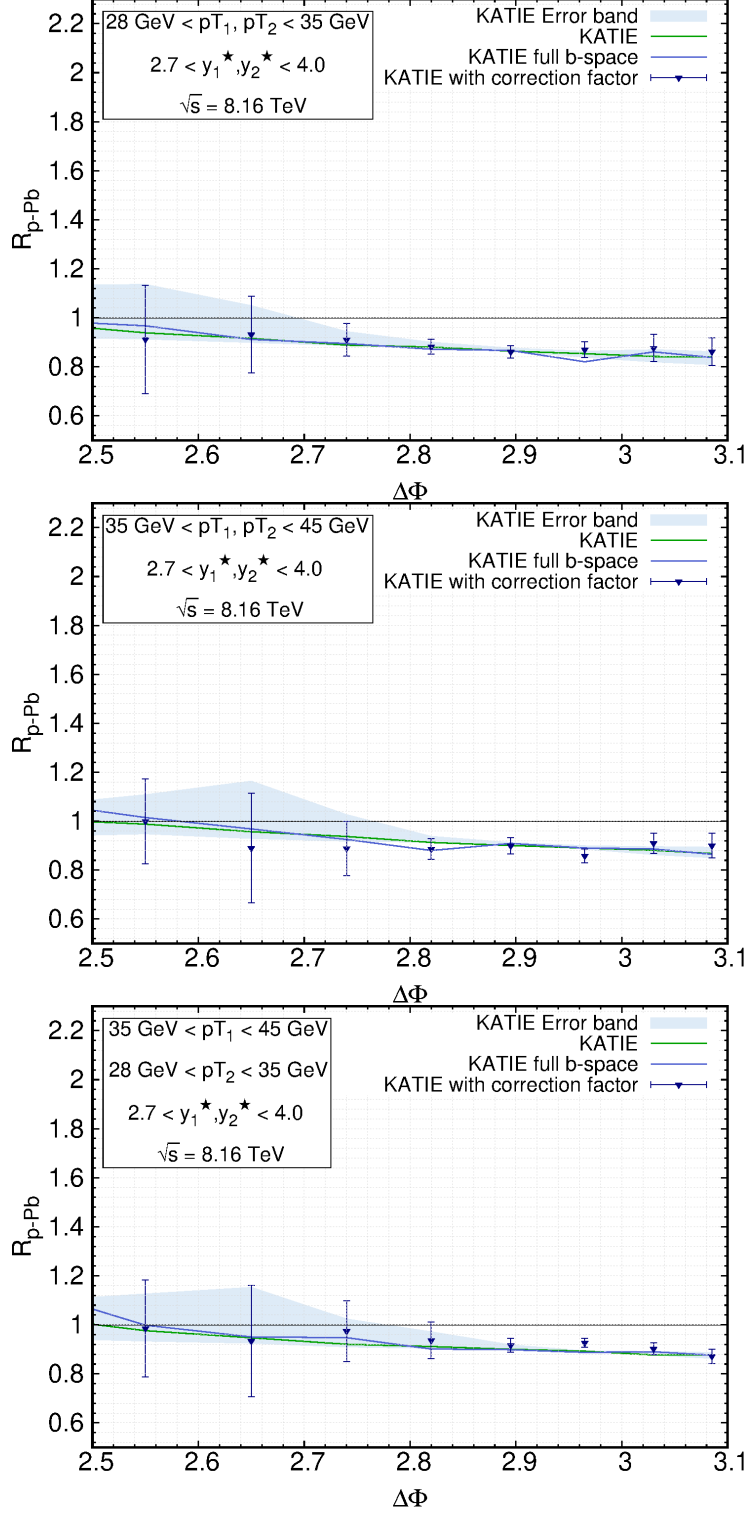


Figure 14: Nuclear modification ratio R_{p-Pb} in terms of the azimuthal angle $\Delta\phi$ between the leading and the sub-leading jets for the proton-proton and the proton-lead collisions at $\sqrt{s} = 8.16$ TeV in the FCal ATLAS kinematics. The solid lines represent the results from KATIE computed within the ITMD approach with: the simplified Sudakov resummation Eq. (42) (red line), the full b -space resummation Eq. (62) (blue line). The band represents the error due to the variation of the factorization/renormalization scales from a value of $(p_{T1} + p_{T2})/2$ by a factor of $1/2$ and 2 . The points ∇ represent the KATIE results corrected with the non-perturbative correction factor extracted from PYTHIA. The error bars associated with these points account for both errors due to variation of scale in KATIE and the statistical uncertainties in the correction factor from PYTHIA. The plots were taken from [197].

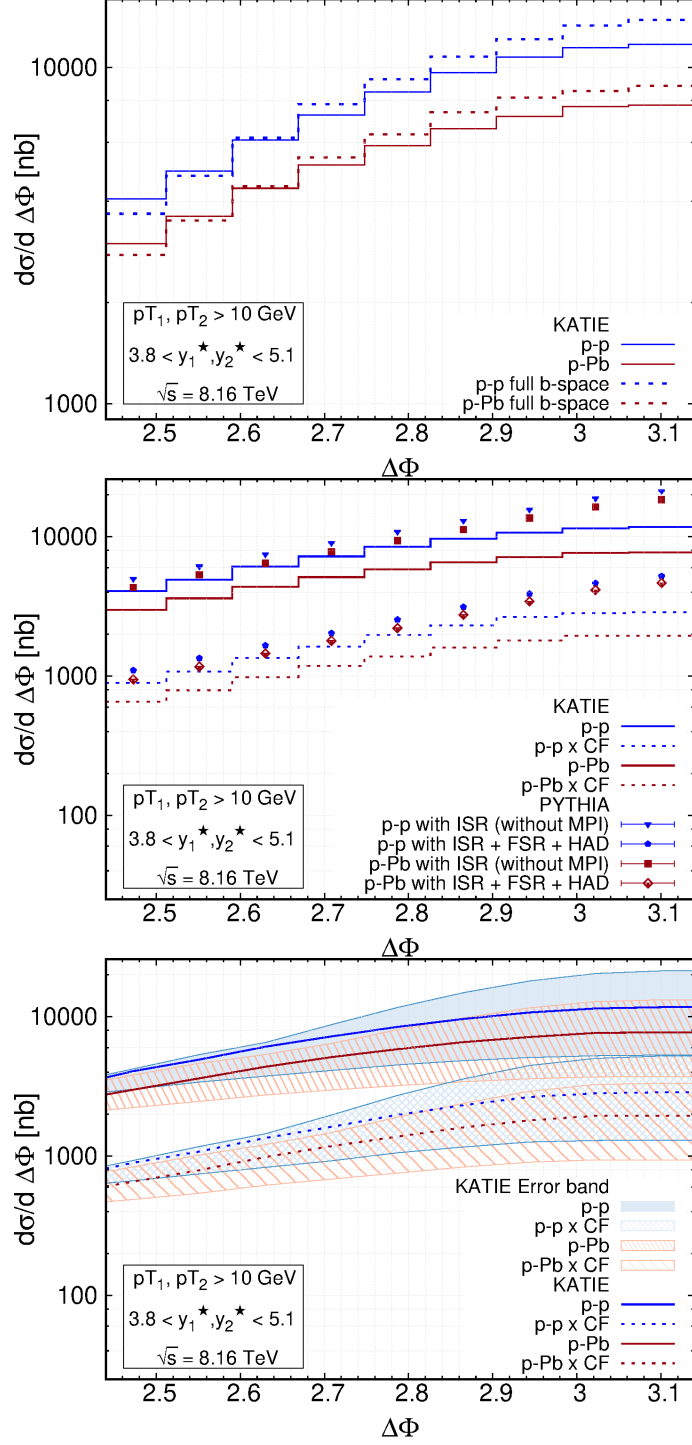


Figure 15: The differential cross sections in terms of the azimuthal angle $\Delta\phi$ between the leading and the sub-leading jets for the proton-proton and the proton-lead collisions at $\sqrt{s} = 8.16$ TeV in the ALICE FoCal kinematics. The first plot represents the cross sections computed using KATIE within the ITMD factorization formula with: the simplified Sudakov resummation Eq. (42) (solid lines), the full b -space resummation Eq. (62) (dotted lines). In the second plot, the solid lines represent the cross sections from KATIE computed within the ITMD approach, the points represent the results from PYTHIA with different components, and the dotted lines represent the KATIE results corrected with the non-perturbative correction factor extracted from PYTHIA. In the third plot, the solid lines represent the cross sections from KATIE computed within the ITMD approach, and the dotted lines represent the KATIE results corrected with the non-perturbative correction factor extracted from PYTHIA. The bands represent the error due to the variation of the factorization/renormalization scales in KATIE from a value of $(p_{T1} + p_{T2})/2$ by a factor of 1/2 and 2. The plots were taken from [197].

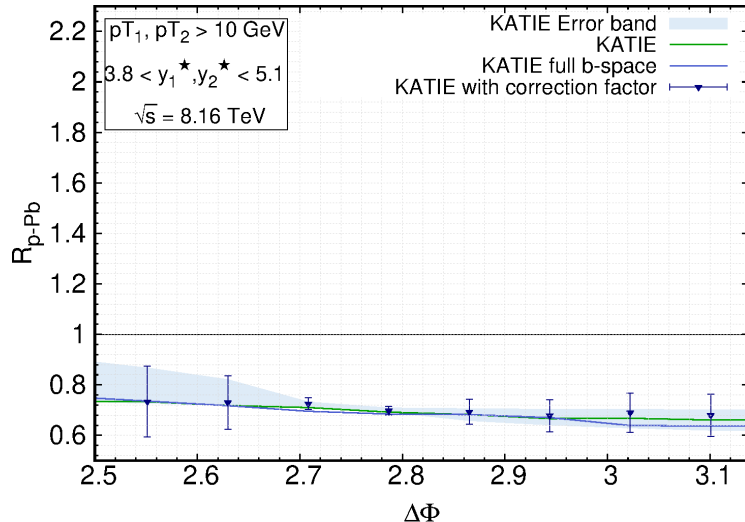


Figure 16: Nuclear modification ratio R_{p-Pb} in terms of the azimuthal angle $\Delta\phi$ between the leading and the sub-leading jets for the proton-proton and the proton-lead collisions at $\sqrt{s} = 8.16$ TeV in the ALICE FoCal kinematics. The solid lines represent the results from KATIE computed within the ITMD approach with: the simplified Sudakov resummation Eq. (42) (red line), the full b -space resummation Eq. (62) (blue line). The band represents the error due to the variation of the factorization/renormalization scales from a value of $(p_{T1} + p_{T2})/2$ by a factor of 1/2 and 2. The points ∇ represent the KATIE results corrected with the non-perturbative correction factor extracted from PYTHIA. The error bars associated with these points account for both errors due to variation of scale in KATIE and the statistical uncertainties in the correction factor from PYTHIA. The plots were taken from [197].

4.8 Forward dijets at Electron Ion Collider

While the focus of this review is on forward jets at LHC, the new accelerator Electron Ion Collider (EIC) is just around the corner [29]. A vital part of its research program is to look for gluon saturation. However, since the involved hard scales are lower than at the LHC, in fact, hadrons constitute better probes of the saturation physics than jets. Nevertheless, there has been a large interest in jets at EIC, see for example [173, 204, 205]. Moreover, at the partonic level, both hadron and jet production need classes of the same diagrams. Therefore, the upcoming EIC experiment triggered tremendous progress in computing NLO corrections for the DIS process within the CGC formalism, see for example [94, 99, 132, 137, 206, 207].

In the context of the ITMD factorization, dijet production at EIC is actually a very interesting and important process. As discussed e.g. in [157] the only TMD gluon distribution that is relevant for dijets in DIS, in the back-to-back limit, is the Weizsacker-Williams (WW) gluon distribution $F_{gg}^{(3)}$ (called also $xG^{(1)}$)². For the ITMD factorization, this is only true for sufficiently small photon virtuality $Q^2 \ll p_T$, otherwise longitudinally polarized gluons contribute, and they are not formally accounted for in the ITMD approach. Due to this fact, for processes where such contributions formally enter, the ITMD factorization is called ITMD* (see for example [174] for the trijet production case).

The dijet production in the DIS process gives actually more interesting observables than dijets in hadron-hadron scattering. This is because there is also an identified electron in the final state. Thus, in addition to dijet azimuthal correlations, one can also study correlations with the outgoing electron.

The ITMD* factorization formula for the process

$$A(P_A) + e^-(P_B) \rightarrow J(p_1) + J(p_2) + e^-(P'_B) + X, \quad (82)$$

²This distribution is also probed in forward Ultra Peripheral Collisions at LHC. We however do not discuss this process here. First application of ITMD to UPC processes can be found in [208]

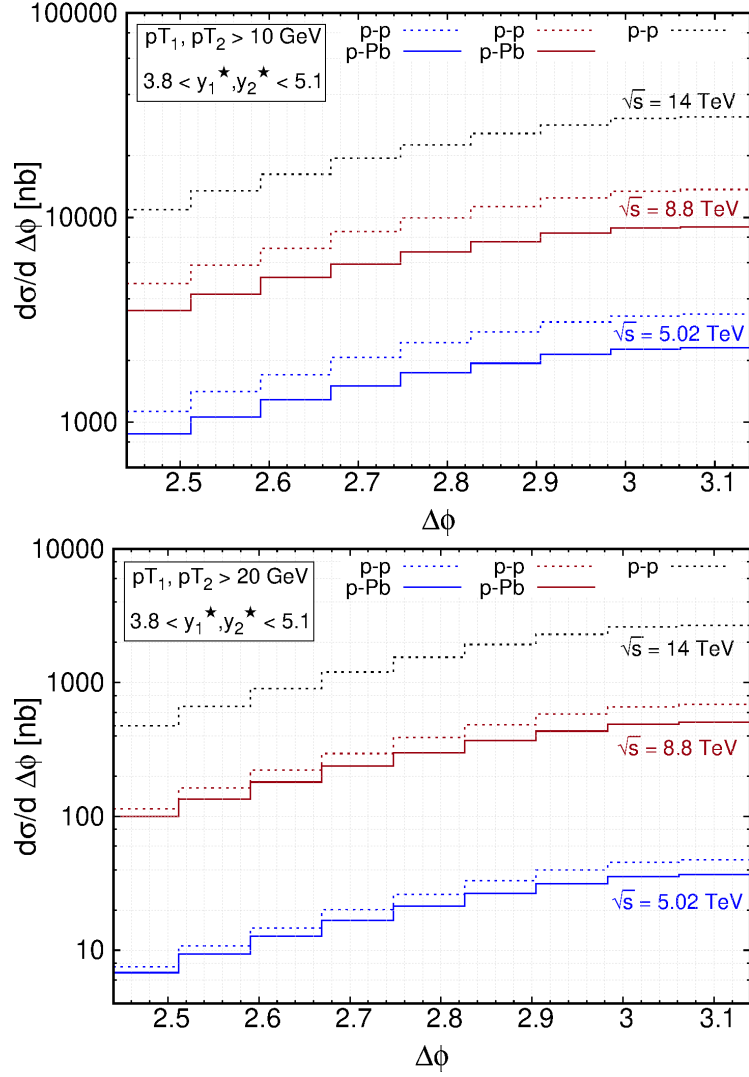


Figure 17: The differential cross sections in terms of the azimuthal angle $\Delta\phi$ between the leading and the sub-leading jets for the proton-proton and the proton-lead collisions at $\sqrt{s} = 5.02$ TeV (blue) and 8.8 TeV (red) in the ALICE FoCal kinematics. For the same kinematics, each plot also represents the differential cross section for the proton-proton collision at $\sqrt{s} = 5.02$ TeV (black). Since proton-lead collisions are not feasible at this energy, we didn't compute those. All of these cross sections were computed using KATIE within the ITMD factorization formula with the simplified Sudakov resummation Eq. (42). The solid lines represent the results for proton-lead collisions and the dotted lines represent the results for the proton-proton collisions.

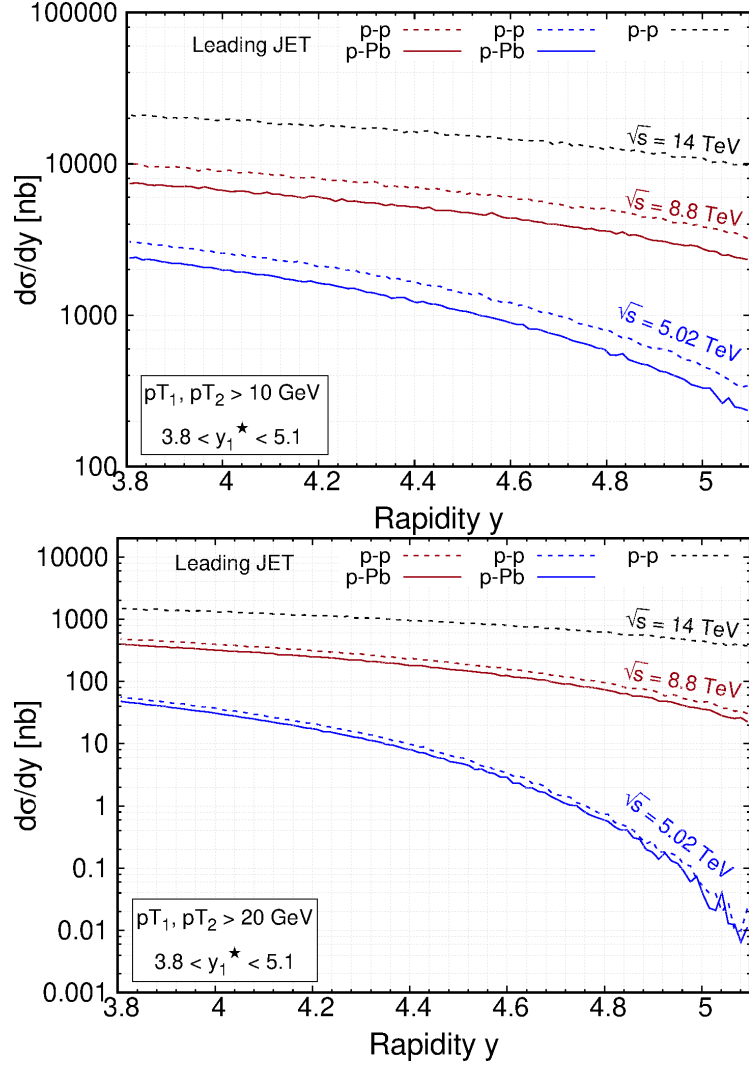


Figure 18: The differential cross sections in terms of the rapidity of the leading jet y_1^* for the proton-proton and the proton-lead collisions at $\sqrt{s} = 5.02$ TeV (blue) and 8.8 TeV (red) in the ALICE FoCal kinematics. For the same kinematics, each plot also represents the differential cross section for the proton-proton collision at $\sqrt{s} = 5.02$ TeV (black). Since proton-lead collisions are not feasible at this energy, we didn't compute those. All of these cross sections were computed using KATIE within the ITMD factorization formula with the simplified Sudakov resummation Eq. (42) The solid lines represent the results for proton-lead collisions and the dotted lines represent the results for the proton-proton collisions.

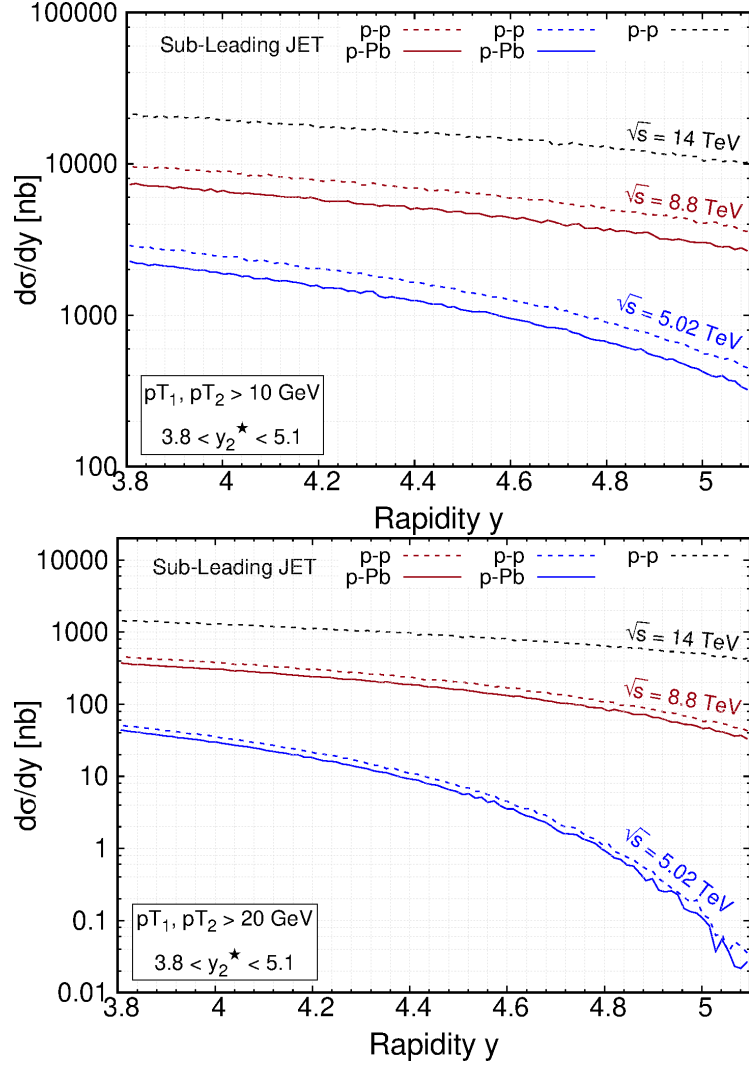


Figure 19: The differential cross sections in terms of the rapidity of the sub-leading jet y_2^* for the proton-proton and the proton-lead collisions at $\sqrt{s} = 5.02$ TeV (blue) and 8.8 TeV (red) in the ALICE FoCal kinematics. For the same kinematics, each plot also represents the differential cross section for the proton-proton collision at $\sqrt{s} = 5.02$ TeV (black). Since proton-lead collisions are not feasible at this energy, we didn't compute those. All of these cross sections were computed using KATIE within the ITMD factorization formula with the simplified Sudakov resummation Eq. (42). The solid lines represent the results for proton-lead collisions and the dotted lines represent the results for the proton-proton collisions.

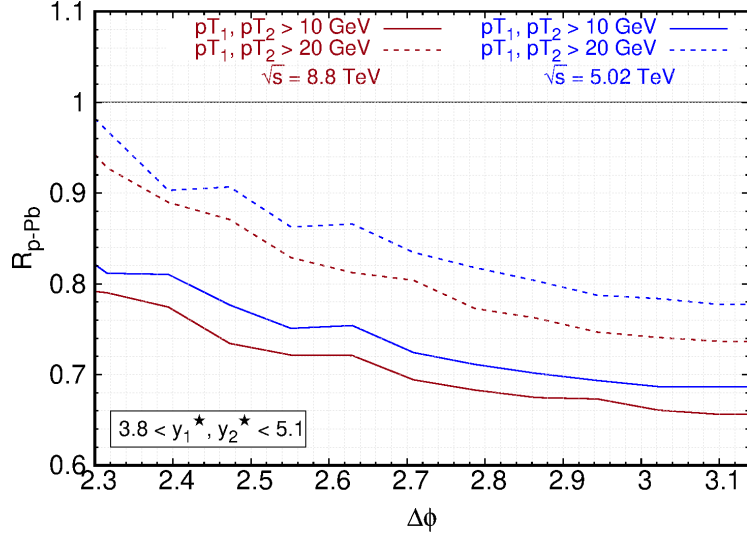


Figure 20: Nuclear modification ratio R_{p-Pb} in terms of the azimuthal angle $\Delta\phi$ between the leading and the sub-leading jets for the proton-proton and the proton-lead collisions at $\sqrt{s} = 5.02$ TeV (blue) and 8.8 TeV (red) in the ALICE FoCal kinematics. The solid lines represent the results from KATIE computed within the ITMD approach with the simplified Sudakov resummation Eq. (42) for $p_{T1}, p_{T2} > 10$ GeV. And the dotted lines represent the results for $p_{T1}, p_{T2} > 20$ GeV.

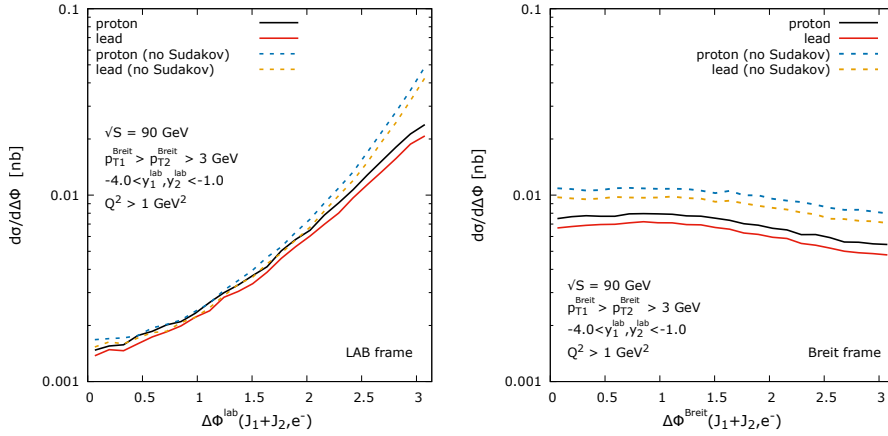


Figure 21: Azimuthal correlations between the total transverse momentum of the dijet system and the transverse momentum of the scattered electron at EIC in two frames: the LAB frame (left), the Breit frame (right). The calculation has been done within the ITMD* framework with the Weizsäcker-Williams gluon distribution obtained from the Kutak-Sapeta fit to HERA data.

reads

$$d\sigma_{eA \rightarrow e' + 2j + X} = \int \frac{dx_A}{x_A} d^2k_T \frac{1}{4\pi x_A P_A \cdot P_B} \mathcal{F}_{gg}^{(3)}(x_A, |\vec{k}_T|, \mu) |\overline{M}_{eg^* \rightarrow e' + 2j}|^2 d\Gamma_3. \quad (83)$$

As mentioned above, there is only WW gluon distribution in the above formula.

In [209] we computed several observables using the above framework, not only to quantify possible saturation effects in dijet observable at EIC but also to demonstrate the relevance of interplay of the saturation, the Sudakov effect, and the exact kinematics.

First, we found that in the context of saturation physics, it is best to consider forward dijets. This provides a very good focusing of the x_A distribution around the sufficiently small values so that the use of the small- x formalism is well justified. For the WW gluon distribution, we used the Kutak-Sapeta fit of the dipole TMD to HERA data, and then the WW TMD distribution was calculated in the mean field approximation (see Section 4.5). The calculation was supplemented with the Sudakov form factor, see Fig. 9 and the corresponding discussion in the text. In Fig. 21 we show prediction for the cross section dependence on azimuthal angle between the dijet system and the scattered electron for CM energy per nucleon $\sqrt{s} = 90$ GeV. The calculations are done both in the lab frame and the Breit frame. One clearly sees effects coming from the Sudakov form factor while the saturation is rather mild, despite the cut on the jet transverse momentum (in the Breit frame) is very low. Primarily, it is a consequence of the saturation pattern visible in the WW gluon distribution. Unlike the dipole gluon distribution, it does not have a peak as a function of the transverse momentum, *c.f.* Fig. 9 and 8. In our computation, we put quite a low cut on the photon virtuality $Q^2 > 1$ GeV² in order to suppress the longitudinal gluons. For a complete discussion see [209] and [210].

5 Summary and outlook

The text discusses the challenges and selected ongoing research related to searches of gluon saturation in QCD using dijet observables. Although there are indications of saturation in the experimental data, achieving a complete consensus on its existence is still a challenge due to demanding kinematics and the complex collision environment. While there are simpler observables than dijets, the latter have the advantage of providing the azimuthal correlations, which in the back-to-back kinematics are sensitive to saturation even for relatively hard jets.

The study of forward dijet production, using the Improved TMD Factorization (ITMD) framework, is a relatively novel proposal in the search for gluon saturation. The framework has been already used in addressing many dijet related observables that were reviewed in this work. The text highlights the need for more measurements and the construction of the FoCal detector by the ALICE collaboration to shed more light on the saturation phenomenon. Furthermore, it discusses complementary dijet measurements in photon nucleus scattering that can be done at the Electron Ion Collider.

While in the review we focused our attention on dijets, there are other forward physics final states that can be used to search for saturation effects [211]. Those include di-hadrons [13, 212, 213], J/ψ production [214], and trijets [140, 174]. The processes are complementary to dijets, however, in some aspects more challenging. The di-hadrons require knowledge of fragmentation function and are sensitive to longitudinal polarization effects while trijets are just more difficult to measure and interpret.

The future research will be focused on increasing the precision of the calculations. The ITMD framework is well suited to extrapolate methods known in collinear factorization to compute higher order corrections to off-shell gauge invariant matrix elements, and in principle to automatize NLO computations. First steps toward that goal have already been undertaken [215–218]. Also, it is important to increase the accuracy of the evolution equations and there is also a substantial progress in this direction, see for example [105, 167, 219–225]. Last but not least, the ITMD framework should account for the longitudinally polarized gluons, which contribute to some processes (see eg. [226]). The corresponding amplitudes should be obtainable automatically, similarly to off-shell gauge invariant amplitudes coupled eikonally that are used currently in the ITMD. Research in that direction is also ongoing.

6 Acknowledgements

We would like to thank Jacek Otwinowski for interesting and stimulating discussions.

HK is supported by the National Science Centre, Poland grant no. DEC-2021/41/N/ST2/02956.

PK is partially supported by the National Science Centre, Poland grant no. DEC-2020/39/O/ST2/03011.

KK acknowledges the Polish National Science Centre grant no. DEC-2017/27/B/ST2/01985.

AvH is supported by the National Science Centre, Poland grant no. DEC-2019/35/B/ST2/03531

References

- [1] L. Gribov, E. Levin and M. Ryskin, *Semihard Processes in QCD*, *Phys. Rept.* **100** (1983) 1–150.
- [2] A. H. Mueller and J.-w. Qiu, *Gluon Recombination and Shadowing at Small Values of x* , *Nucl. Phys. B* **268** (1986) 427–452.
- [3] E. Iancu and R. Venugopalan, *The Color glass condensate and high-energy scattering in QCD*, pp. 249–3363. 3, 2003. [hep-ph/0303204](#). 10.1142/9789812795533_0005.
- [4] J. Jalilian-Marian and Y. V. Kovchegov, *Saturation physics and deuteron-Gold collisions at RHIC*, *Prog. Part. Nucl. Phys.* **56** (2006) 104–231, [[hep-ph/0505052](#)].
- [5] F. Gelis, E. Iancu, J. Jalilian-Marian and R. Venugopalan, *The Color Glass Condensate*, *Ann. Rev. Nucl. Part. Sci.* **60** (2010) 463–489, [[1002.0333](#)].
- [6] J. L. Albacete and C. Marquet, *Gluon saturation and initial conditions for relativistic heavy ion collisions*, *Prog. Part. Nucl. Phys.* **76** (2014) 1–42, [[1401.4866](#)].
- [7] J.-P. Blaizot, *High gluon densities in heavy ion collisions*, *Rept. Prog. Phys.* **80** (2017) 032301, [[1607.04448](#)].
- [8] Y. V. Kovchegov and E. Levin, *Quantum chromodynamics at high energy*, vol. 33. Cambridge University Press, 8, 2012, [10.1017/CBO9781139022187](#).
- [9] K. J. Golec-Biernat and M. Wusthoff, *Saturation effects in deep inelastic scattering at low Q^{*2} and its implications on diffraction*, *Phys. Rev. D* **59** (1998) 014017, [[hep-ph/9807513](#)].
- [10] J. L. Albacete and C. Marquet, *Azimuthal correlations of forward di-hadrons in d+Au collisions at RHIC in the Color Glass Condensate*, *Phys. Rev. Lett.* **105** (2010) 162301, [[1005.4065](#)].
- [11] K. Dusling and R. Venugopalan, *Evidence for BFKL and saturation dynamics from dihadron spectra at the LHC*, *Phys. Rev. D* **87** (2013) 051502, [[1210.3890](#)].
- [12] K. Kutak and S. Sapeta, *Gluon saturation in dijet production in p-Pb collisions at Large Hadron Collider*, *Phys. Rev. D* **86** (2012) 094043, [[1205.5035](#)].
- [13] A. Stasto, S.-Y. Wei, B.-W. Xiao and F. Yuan, *On the Dihadron Angular Correlations in Forward pA collisions*, *Phys. Lett. B* **784** (2018) 301–306, [[1805.05712](#)].
- [14] A. van Hameren, P. Kotko, K. Kutak and S. Sapeta, *Broadening and saturation effects in dijet azimuthal correlations in p-p and p-Pb collisions at $\sqrt{s} = 5.02$ TeV*, *Phys. Lett. B* **795** (2019) 511–515, [[1903.01361](#)].
- [15] H. Mäntysaari and H. Paukkunen, *Saturation and forward jets in proton-lead collisions at the LHC*, *Phys. Rev. D* **100** (2019) 114029, [[1910.13116](#)].
- [16] B. Ducloué, E. Iancu, G. Soyez and D. N. Triantafyllopoulos, *HERA data and collinearly-improved BK dynamics*, *Phys. Lett. B* **803** (2020) 135305, [[1912.09196](#)].

- [17] A. Arroyo Garcia, M. Hentschinski and K. Kutak, *QCD evolution based evidence for the onset of gluon saturation in exclusive photo-production of vector mesons*, *Phys. Lett. B* **795** (2019) 569–575, [[1904.04394](#)].
- [18] STAR collaboration, M. S. Abdallah et al., *Evidence for Nonlinear Gluon Effects in QCD and Their Mass Number Dependence at STAR*, *Phys. Rev. Lett.* **129** (2022) 092501, [[2111.10396](#)].
- [19] G. Beuf, H. Hänninen, T. Lappi and H. Mäntysaari, *Color Glass Condensate at next-to-leading order meets HERA data*, *Phys. Rev. D* **102** (2020) 074028, [[2007.01645](#)].
- [20] A. Morreale and F. Salazar, *Mining for Gluon Saturation at Colliders*, *Universe* **7** (2021) 312, [[2108.08254](#)].
- [21] M. Cacciari, J. Rojo, G. P. Salam and G. Soyez, *Jet Reconstruction in Heavy Ion Collisions*, *Eur. Phys. J. C* **71** (2011) 1539, [[1010.1759](#)].
- [22] C. Marquet, *Forward inclusive dijet production and azimuthal correlations in $p(A)$ collisions*, *Nucl. Phys. A* **796** (2007) 41–60, [[0708.0231](#)].
- [23] A. van Hameren, P. Kotko, K. Kutak, C. Marquet and S. Sapeta, *Saturation effects in forward-forward dijet production in $p+Pb$ collisions*, *Phys. Rev. D* **89** (2014) 094014, [[1402.5065](#)].
- [24] K. Kutak, *Hard scale dependent gluon density, saturation and forward-forward dijet production at the LHC*, *Phys. Rev. D* **91** (2015) 034021, [[1409.3822](#)].
- [25] ATLAS collaboration, M. Aaboud et al., *Dijet azimuthal correlations and conditional yields in pp and $p+Pb$ collisions at $s_{NN}=5.02\text{TeV}$ with the ATLAS detector*, *Phys. Rev. C* **100** (2019) 034903, [[1901.10440](#)].
- [26] CMS collaboration, A. M. Sirunyan et al., *Measurement of inclusive very forward jet cross sections in proton-lead collisions at $\sqrt{s_{NN}} = 5.02\text{ TeV}$* , *JHEP* **05** (2019) 043, [[1812.01691](#)].
- [27] C. ALICE Collaboration, *Letter of Intent: A Forward Calorimeter (FoCal) in the ALICE experiment*, tech. rep., CERN, Geneva, Jun, 2020.
- [28] A. Accardi et al., *Electron Ion Collider: The Next QCD Frontier: Understanding the glue that binds us all*, *Eur. Phys. J. A* **52** (2016) 268, [[1212.1701](#)].
- [29] R. Abdul Khalek et al., *Science Requirements and Detector Concepts for the Electron-Ion Collider: EIC Yellow Report*, *Nucl. Phys. A* **1026** (2022) 122447, [[2103.05419](#)].
- [30] P. Kotko, K. Kutak, C. Marquet, E. Petreska, S. Sapeta and A. van Hameren, *Improved TMD factorization for forward dijet production in dilute-dense hadronic collisions*, *JHEP* **09** (2015) 106, [[1503.03421](#)].
- [31] J. Collins, *Foundations of perturbative QCD*, vol. 32. Cambridge University Press, 11, 2013.
- [32] ATLAS collaboration, G. Aad et al., *Measurement of Dijet Azimuthal Decorrelations in pp Collisions at $\sqrt{s} = 7\text{ TeV}$* , *Phys. Rev. Lett.* **106** (2011) 172002, [[1102.2696](#)].
- [33] CMS collaboration, V. Khachatryan et al., *Dijet Azimuthal Decorrelations in pp Collisions at $\sqrt{s} = 7\text{ TeV}$* , *Phys. Rev. Lett.* **106** (2011) 122003, [[1101.5029](#)].
- [34] M. Bonvini, *Small- x resummation in PDF fits and future prospects*, in *Diffraction and Low- x 2022*, 12, 2022. [2212.14231](#).
- [35] M. Froissart, *Asymptotic behavior and subtractions in the Mandelstam representation*, *Phys. Rev.* **123** (1961) 1053–1057.

- [36] J. Bartels, K. Golec-Biernat and L. Motyka, *Twist expansion of the nucleon structure functions, $F(2)$ and $F(L)$, in the DGLAP improved saturation model*, *Phys. Rev. D* **81** (2010) 054017, [[0911.1935](#)].
- [37] L. Motyka, M. Sadzikowski and W. Slominski, *Evidence of strong higher twist effects in diffractive DIS at HERA at moderate Q^2* , *Phys. Rev. D* **86** (2012) 111501, [[1203.5461](#)].
- [38] L. Motyka and M. Sadzikowski, *Twist decomposition of proton structure from BFKL and BK amplitudes*, *Acta Phys. Polon. B* **45** (2014) 2079, [[1411.7774](#)].
- [39] L. Motyka, M. Sadzikowski and T. Stebel, *Twist expansion of Drell-Yan structure functions in color dipole approach*, *JHEP* **05** (2015) 087, [[1412.4675](#)].
- [40] D. Brzemiński, L. Motyka, M. Sadzikowski and T. Stebel, *Twist decomposition of Drell-Yan structure functions: phenomenological implications*, *JHEP* **01** (2017) 005, [[1611.04449](#)].
- [41] L. Motyka, M. Sadzikowski, W. Słomiński and K. Wichmann, *Evidence of quasi-partonic higher-twist effects in deep inelastic scattering at HERA at moderate Q^2* , *Eur. Phys. J. C* **78** (2018) 80, [[1707.05992](#)].
- [42] H. D. I. Abarbanel, J. B. Bronzan, R. L. Sugar and A. R. White, *Reggeon Field Theory: Formulation and Use*, *Phys. Rept.* **21** (1975) 119–182.
- [43] J. Bartels, C. Contreras and G. P. Vacca, *Could reggeon field theory be an effective theory for QCD in the Regge limit?*, *JHEP* **03** (2016) 201, [[1512.07182](#)].
- [44] A. Kovner, E. Levin, M. Li and M. Lublinsky, *The JIMWLK evolution and the s-channel unitarity*, *JHEP* **09** (2020) 199, [[2006.15126](#)].
- [45] A. Kovner, E. Levin, M. Li and M. Lublinsky, *Reggeon Field Theory and Self Duality: Making Ends Meet*, *JHEP* **10** (2020) 185, [[2007.12132](#)].
- [46] I. Balitsky and L. Lipatov, *The Pomeron Singularity in Quantum Chromodynamics*, *Sov. J. Nucl. Phys.* **28** (1978) 822–829.
- [47] E. A. Kuraev, L. N. Lipatov and V. S. Fadin, *Multi - Reggeon Processes in the Yang-Mills Theory*, *Sov. Phys. JETP* **44** (1976) 443–450.
- [48] E. A. Kuraev, L. N. Lipatov and V. S. Fadin, *The Pomeron Singularity in Nonabelian Gauge Theories*, *Sov. Phys. JETP* **45** (1977) 199–204.
- [49] V. S. Fadin, E. Kuraev and L. Lipatov, *On the Pomeron Singularity in Asymptotically Free Theories*, *Phys. Lett. B* **60** (1975) 50–52.
- [50] J. R. Forshaw and D. A. Ross, *Quantum Chromodynamics and the Pomeron*, vol. 9. Oxford University Press, 1998, [10.1017/9781009290111](#).
- [51] J. Bartels and M. Wusthoff, *The Triple Regge limit of diffractive dissociation in deep inelastic scattering*, *Z. Phys. C* **66** (1995) 157–180.
- [52] J. Bartels, *Unitarity corrections to the Lipatov pomeron and the four gluon operator in deep inelastic scattering in QCD*, *Z. Phys. C* **60** (1993) 471–488.
- [53] J. Bartels and K. Kutak, *A Momentum Space Analysis of the Triple Pomeron Vertex in pQCD*, *Eur. Phys. J. C* **53** (2008) 533–548, [[0710.3060](#)].
- [54] R. Engel, *Photoproduction within the two component dual parton model. 1. Amplitudes and cross-sections*, *Z. Phys. C* **66** (1995) 203–214.
- [55] S. Roesler, R. Engel and J. Ranft, *The Monte Carlo event generator DPMJET-III*, in *International Conference on Advanced Monte Carlo for Radiation Physics, Particle Transport Simulation and Applications (MC 2000)*, pp. 1033–1038, 12, 2000. [hep-ph/0012252](#). DOI.

- [56] K. Werner, F.-M. Liu and T. Pierog, *Parton ladder splitting and the rapidity dependence of transverse momentum spectra in deuteron-gold collisions at RHIC*, *Phys. Rev. C* **74** (2006) 044902, [[hep-ph/0506232](#)].
- [57] K. Werner, *On a deep connection between factorization and saturation: new insight into modeling high-energy proton-proton and nucleus-nucleus scattering in the EPOS4 framework*, [2301.12517](#).
- [58] R. S. Fletcher, T. K. Gaisser, P. Lipari and T. Stanev, *SIBYLL: An Event generator for simulation of high-energy cosmic ray cascades*, *Phys. Rev. D* **50** (1994) 5710–5731.
- [59] E.-J. Ahn, R. Engel, T. K. Gaisser, P. Lipari and T. Stanev, *Cosmic ray interaction event generator SIBYLL 2.1*, *Phys. Rev. D* **80** (2009) 094003, [[0906.4113](#)].
- [60] N. N. Kalmykov, S. S. Ostapchenko and A. I. Pavlov, *Quark-Gluon String Model and EAS Simulation Problems at Ultra-High Energies*, *Nucl. Phys. B Proc. Suppl.* **52** (1997) 17–28.
- [61] S. Ostapchenko, *Monte Carlo treatment of hadronic interactions in enhanced Pomeron scheme: I. QGSJET-II model*, *Phys. Rev. D* **83** (2011) 014018, [[1010.1869](#)].
- [62] L. Lipatov, *Gauge invariant effective action for high-energy processes in QCD*, *Nucl. Phys. B* **452** (1995) 369–400, [[hep-ph/9502308](#)].
- [63] E. Antonov, L. Lipatov, E. Kuraev and I. Cherednikov, *Feynman rules for effective Regge action*, *Nucl. Phys. B* **721** (2005) 111–135, [[hep-ph/0411185](#)].
- [64] M. Hentschinski, *Chapter 11: Lipatov’s QCD High Energy Effective Action: Past and Future*, pp. 283–310. 2021. [2010.14748](#). [10.1142/9789811231124_0011](#).
- [65] J. Bartels, V. Fadin, E. Levin, A. Levy, V. Kim and A. Sabio-Vera, eds., *From the Past to the Future*. World Scientific, 12, 2021, [10.1142/12127](#).
- [66] G. Chachamis, M. Hentschinski, J. D. Madrigal Martínez and A. Sabio Vera, *Quark contribution to the gluon Regge trajectory at NLO from the high energy effective action*, *Nucl. Phys. B* **861** (2012) 133–144, [[1202.0649](#)].
- [67] G. Chachamis, M. Hentschinski, J. D. Madrigal Martínez and A. Sabio Vera, *Forward jet production \(\mathcal{E}\) quantum corrections to the gluon Regge trajectory from Lipatov’s high energy effective action*, *Phys. Part. Nucl.* **45** (2014) 788–799, [[1211.2050](#)].
- [68] G. Chachamis, M. Hentschinski, J. D. Madrigal Martínez and A. Sabio Vera, *Next-to-leading order corrections to the gluon-induced forward jet vertex from the high energy effective action*, *Phys. Rev. D* **87** (2013) 076009, [[1212.4992](#)].
- [69] G. Chachamis, M. Hentschinski, J. D. Madrigal Martínez and A. Sabio Vera, *Gluon Regge trajectory at two loops from Lipatov’s high energy effective action*, *Nucl. Phys. B* **876** (2013) 453–472, [[1307.2591](#)].
- [70] M. Hentschinski, J. D. Madrigal Martínez, B. Murdaca and A. Sabio Vera, *The next-to-leading order vertex for a forward jet plus a rapidity gap at high energies*, *Phys. Lett. B* **735** (2014) 168–172, [[1404.2937](#)].
- [71] S. Bondarenko, L. Lipatov and A. Prygarin, *Effective action for reggeized gluons, classical gluon field of relativistic color charge and color glass condensate approach*, *Eur. Phys. J. C* **77** (2017) 527, [[1706.00278](#)].
- [72] M. Hentschinski, *Color glass condensate formalism, Balitsky-JIMWLK evolution, and Lipatov’s high energy effective action*, *Phys. Rev. D* **97** (2018) 114027, [[1802.06755](#)].
- [73] S. Bondarenko, L. Lipatov, S. Pozdnyakov and A. Prygarin, *One loop light-cone QCD, effective action for reggeized gluons and QCD RFT calculus*, *Eur. Phys. J. C* **77** (2017) 630, [[1708.05183](#)].

- [74] S. Bondarenko and S. Pozdnyakov, *On correlators of Reggeon fields and operators of Wilson lines in high energy QCD*, *Int. J. Mod. Phys. A* **33** (2018) 1850204, [[1806.02563](#)].
- [75] I. Balitsky, *Operator expansion for high-energy scattering*, *Nucl. Phys. B* **463** (1996) 99–160, [[hep-ph/9509348](#)].
- [76] Y. V. Kovchegov, *Small x $F(2)$ structure function of a nucleus including multiple pomeron exchanges*, *Phys. Rev. D* **60** (1999) 034008, [[hep-ph/9901281](#)].
- [77] A. H. Mueller, *Soft gluons in the infinite momentum wave function and the BFKL pomeron*, *Nucl. Phys. B* **415** (1994) 373–385.
- [78] Y. V. Kovchegov, *Unitarization of the BFKL pomeron on a nucleus*, *Phys. Rev. D* **61** (2000) 074018, [[hep-ph/9905214](#)].
- [79] E. Levin and K. Tuchin, *Solution to the evolution equation for high parton density QCD*, *Nucl. Phys. B* **573** (2000) 833–852, [[hep-ph/9908317](#)].
- [80] E. Levin and K. Tuchin, *New scaling at high-energy DIS*, *Nucl. Phys. A* **691** (2001) 779–790, [[hep-ph/0012167](#)].
- [81] E. Levin and K. Tuchin, *Nonlinear evolution and saturation for heavy nuclei in DIS*, *Nucl. Phys. A* **693** (2001) 787–798, [[hep-ph/0101275](#)].
- [82] M. Braun, *Structure function of the nucleus in the perturbative QCD with $N(c) \rightarrow$ infinity (BFKL pomeron fan diagrams)*, *Eur. Phys. J. C* **16** (2000) 337–347, [[hep-ph/0001268](#)].
- [83] N. Armesto and M. A. Braun, *Parton densities and dipole cross-sections at small x in large nuclei*, *Eur. Phys. J. C* **20** (2001) 517–522, [[hep-ph/0104038](#)].
- [84] M. Lublinsky, E. Gotsman, E. Levin and U. Maor, *Nonlinear evolution and parton distributions at LHC and THERA energies*, *Nucl. Phys. A* **696** (2001) 851–869, [[hep-ph/0102321](#)].
- [85] M. Lublinsky, *Scaling phenomena from nonlinear evolution in high-energy DIS*, *Eur. Phys. J. C* **21** (2001) 513–519, [[hep-ph/0106112](#)].
- [86] K. J. Golec-Biernat, L. Motyka and A. M. Stasto, *Diffusion into infrared and unitarization of the BFKL pomeron*, *Phys. Rev. D* **65** (2002) 074037, [[hep-ph/0110325](#)].
- [87] K. J. Golec-Biernat and A. M. Stasto, *On solutions of the Balitsky-Kovchegov equation with impact parameter*, *Nucl. Phys. B* **668** (2003) 345–363, [[hep-ph/0306279](#)].
- [88] E. Gotsman, M. Kozlov, E. Levin, U. Maor and E. Naftali, *Towards a new global QCD analysis: Solution to the nonlinear equation at arbitrary impact parameter*, *Nucl. Phys. A* **742** (2004) 55–79, [[hep-ph/0401021](#)].
- [89] T. Ikeda and L. McLerran, *Impact parameter dependence in the Balitsky-Kovchegov equation*, *Nucl. Phys. A* **756** (2005) 385–398, [[hep-ph/0410345](#)].
- [90] J. Berger and A. Stasto, *Numerical solution of the nonlinear evolution equation at small x with impact parameter and beyond the LL approximation*, *Phys. Rev. D* **83** (2011) 034015, [[1010.0671](#)].
- [91] A. H. Rezaeian and I. Schmidt, *Impact-parameter dependent Color Glass Condensate dipole model and new combined HERA data*, *Phys. Rev. D* **88** (2013) 074016, [[1307.0825](#)].
- [92] D. Bendova, J. Cepila, J. G. Contreras and M. Matas, *Solution to the Balitsky-Kovchegov equation with the collinearly improved kernel including impact-parameter dependence*, *Phys. Rev. D* **100** (2019) 054015, [[1907.12123](#)].

- [93] J. Cepila, J. G. Contreras and M. Matas, *Collinearly improved kernel suppresses Coulomb tails in the impact-parameter dependent Balitsky-Kovchegov evolution*, *Phys. Rev. D* **99** (2019) 051502, [[1812.02548](#)].
- [94] T. Altinoluk, G. Beuf, A. Czajka and A. Tymowska, *Quarks at next-to-eikonal accuracy in the CGC: Forward quark-nucleus scattering*, *Phys. Rev. D* **104** (2021) 014019, [[2012.03886](#)].
- [95] G. A. Chirilli, *High-energy operator product expansion at sub-eikonal level*, *JHEP* **06** (2021) 096, [[2101.12744](#)].
- [96] Y. V. Kovchegov and M. G. Santiago, *Quark sivers function at small x : spin-dependent odderon and the sub-eikonal evolution*, *JHEP* **11** (2021) 200, [[2108.03667](#)].
- [97] T. Altinoluk and G. Beuf, *Quark and scalar propagators at next-to-eikonal accuracy in the CGC through a dynamical background gluon field*, *Phys. Rev. D* **105** (2022) 074026, [[2109.01620](#)].
- [98] P. Agostini, T. Altinoluk, N. Armesto, F. Dominguez and J. G. Milhano, *Multiparticle production in proton–nucleus collisions beyond eikonal accuracy*, *Eur. Phys. J. C* **82** (2022) 1001, [[2207.10472](#)].
- [99] T. Altinoluk, G. Beuf, A. Czajka and A. Tymowska, *DIS dijet production at next-to-eikonal accuracy in the CGC*, *Phys. Rev. D* **107** (2023) 074016, [[2212.10484](#)].
- [100] T. Altinoluk, N. Armesto and G. Beuf, *Probing quark transverse momentum distributions in the Color Glass Condensate: quark-gluon dijets in Deep Inelastic Scattering at next-to-eikonal accuracy*, [2303.12691](#).
- [101] I. Balitsky and G. A. Chirilli, *Next-to-leading order evolution of color dipoles*, *Phys. Rev. D* **77** (2008) 014019, [[0710.4330](#)].
- [102] A. Kovner, M. Lublinsky and Y. Mulian, *Jalilian-Marian, Iancu, McLerran, Weigert, Leonidov, Kovner evolution at next to leading order*, *Phys. Rev. D* **89** (2014) 061704, [[1310.0378](#)].
- [103] A. Kovner, M. Lublinsky and Y. Mulian, *NLO JIMWLK evolution unabridged*, *JHEP* **08** (2014) 114, [[1405.0418](#)].
- [104] T. Lappi and H. Mäntysaari, *Direct numerical solution of the coordinate space Balitsky-Kovchegov equation at next to leading order*, *Phys. Rev. D* **91** (2015) 074016, [[1502.02400](#)].
- [105] T. Lappi and H. Mäntysaari, *Next-to-leading order Balitsky-Kovchegov equation with resummation*, *Phys. Rev. D* **93** (2016) 094004, [[1601.06598](#)].
- [106] B. Ducloué, E. Iancu, A. H. Mueller, G. Soyez and D. N. Triantafyllopoulos, *Non-linear evolution in QCD at high-energy beyond leading order*, *JHEP* **04** (2019) 081, [[1902.06637](#)].
- [107] L. D. McLerran and R. Venugopalan, *Computing quark and gluon distribution functions for very large nuclei*, *Phys. Rev. D* **49** (1994) 2233–2241, [[hep-ph/9309289](#)].
- [108] L. D. McLerran and R. Venugopalan, *Gluon distribution functions for very large nuclei at small transverse momentum*, *Phys. Rev. D* **49** (1994) 3352–3355, [[hep-ph/9311205](#)].
- [109] Y. V. Kovchegov, *NonAbelian Weizsacker-Williams field and a two-dimensional effective color charge density for a very large nucleus*, *Phys. Rev. D* **54** (1996) 5463–5469, [[hep-ph/9605446](#)].
- [110] J. Jalilian-Marian, A. Kovner, L. D. McLerran and H. Weigert, *The Intrinsic glue distribution at very small x* , *Phys. Rev. D* **55** (1997) 5414–5428, [[hep-ph/9606337](#)].

- [111] J. Jalilian-Marian, A. Kovner, A. Leonidov and H. Weigert, *The BFKL equation from the Wilson renormalization group*, *Nucl. Phys. B* **504** (1997) 415–431, [[hep-ph/9701284](#)].
- [112] A. Kovner, J. G. Milhano and H. Weigert, *Relating different approaches to nonlinear QCD evolution at finite gluon density*, *Phys. Rev.* **D62** (2000) 114005, [[hep-ph/0004014](#)].
- [113] A. Kovner and J. G. Milhano, *Vector potential versus color charge density in low x evolution*, *Phys. Rev.* **D61** (2000) 014012, [[hep-ph/9904420](#)].
- [114] H. Weigert, *Unitarity at small Bjorken x* , *Nucl. Phys.* **A703** (2002) 823–860, [[hep-ph/0004044](#)].
- [115] E. Iancu, A. Leonidov and L. D. McLerran, *Nonlinear gluon evolution in the color glass condensate. 1.*, *Nucl. Phys.* **A692** (2001) 583–645, [[hep-ph/0011241](#)].
- [116] E. Ferreiro, E. Iancu, A. Leonidov and L. McLerran, *Nonlinear gluon evolution in the color glass condensate. 2.*, *Nucl. Phys. A* **703** (2002) 489–538, [[hep-ph/0109115](#)].
- [117] A. Dumitru, A. Hayashigaki and J. Jalilian-Marian, *The Color glass condensate and hadron production in the forward region*, *Nucl. Phys. A* **765** (2006) 464–482, [[hep-ph/0506308](#)].
- [118] H. Fujii, F. Gelis and R. Venugopalan, *Quark pair production in high energy pA collisions: General features*, *Nucl. Phys. A* **780** (2006) 146–174, [[hep-ph/0603099](#)].
- [119] E. Iancu and J. Laidet, *Gluon splitting in a shockwave*, *Nucl. Phys. A* **916** (2013) 48–78, [[1305.5926](#)].
- [120] G. A. Chirilli, B.-W. Xiao and F. Yuan, *One-loop Factorization for Inclusive Hadron Production in pA Collisions in the Saturation Formalism*, *Phys. Rev. Lett.* **108** (2012) 122301, [[1112.1061](#)].
- [121] G. A. Chirilli, B.-W. Xiao and F. Yuan, *Inclusive Hadron Productions in pA Collisions*, *Phys. Rev. D* **86** (2012) 054005, [[1203.6139](#)].
- [122] A. M. Stasto, B.-W. Xiao and D. Zaslavsky, *Towards the Test of Saturation Physics Beyond Leading Logarithm*, *Phys. Rev. Lett.* **112** (2014) 012302, [[1307.4057](#)].
- [123] B. Ducloué, T. Lappi and Y. Zhu, *Single inclusive forward hadron production at next-to-leading order*, *Phys. Rev. D* **93** (2016) 114016, [[1604.00225](#)].
- [124] E. Iancu, A. H. Mueller and D. N. Triantafyllopoulos, *CGC factorization for forward particle production in proton-nucleus collisions at next-to-leading order*, *JHEP* **12** (2016) 041, [[1608.05293](#)].
- [125] H.-Y. Liu, Y.-Q. Ma and K.-T. Chao, *Improvement for Color Glass Condensate factorization: single hadron production in pA collisions at next-to-leading order*, *Phys. Rev. D* **100** (2019) 071503, [[1909.02370](#)].
- [126] H.-y. Liu, K. Xie, Z. Kang and X. Liu, *Single inclusive jet production in pA collisions at NLO in the small- x regime*, *JHEP* **07** (2022) 041, [[2204.03026](#)].
- [127] B. Ducloué, H. Hänninen, T. Lappi and Y. Zhu, *Deep inelastic scattering in the dipole picture at next-to-leading order*, *Phys. Rev. D* **96** (2017) 094017, [[1708.07328](#)].
- [128] G. Beuf, T. Lappi and R. Paatelainen, *Massive quarks in NLO dipole factorization for DIS: Transverse photon*, *Phys. Rev. D* **106** (2022) 034013, [[2204.02486](#)].
- [129] H. Hänninen, H. Mäntysaari, R. Paatelainen and J. Penttala, *Proton Structure Functions at Next-to-Leading Order in the Dipole Picture with Massive Quarks*, *Phys. Rev. Lett.* **130** (2023) 192301, [[2211.03504](#)].
- [130] P. Caucal, F. Salazar and R. Venugopalan, *Dijet impact factor in DIS at next-to-leading order in the Color Glass Condensate*, *JHEP* **11** (2021) 222, [[2108.06347](#)].

- [131] P. Caucal, F. Salazar, B. Schenke and R. Venugopalan, *Back-to-back inclusive dijets in DIS at small x : Sudakov suppression and gluon saturation at NLO*, [2208.13872](#).
- [132] P. Caucal, F. Salazar, B. Schenke, T. Stebel and R. Venugopalan, *Back-to-back inclusive dijets in DIS at small x : Gluon Weizsäcker-Williams distribution at NLO*, [2304.03304](#).
- [133] H. Mäntysaari and J. Penttala, *Exclusive production of light vector mesons at next-to-leading order in the dipole picture*, *Phys. Rev. D* **105** (2022) 114038, [[2203.16911](#)].
- [134] H. Mäntysaari and J. Penttala, *Complete calculation of exclusive heavy vector meson production at next-to-leading order in the dipole picture*, *JHEP* **08** (2022) 247, [[2204.14031](#)].
- [135] E. Iancu and Y. Mulian, *Forward dijets in proton-nucleus collisions at next-to-leading order: the real corrections*, *JHEP* **03** (2021) 005, [[2009.11930](#)].
- [136] E. Iancu and Y. Mulian, *Dihadron production in DIS at NLO: the real corrections*, [2211.04837](#).
- [137] P. Taels, T. Altinoluk, G. Beuf and C. Marquet, *Dijet photoproduction at low x at next-to-leading order and its back-to-back limit*, [2204.11650](#).
- [138] T. Altinoluk, R. Boussarie, C. Marquet and P. Taels, *TMD factorization for dijets + photon production from the dilute-dense CGC framework*, *JHEP* **07** (2019) 079, [[1810.11273](#)].
- [139] E. Iancu and Y. Mulian, *Forward trijet production in proton–nucleus collisions*, *Nucl. Phys. A* **985** (2019) 66–127, [[1809.05526](#)].
- [140] T. Altinoluk, R. Boussarie, C. Marquet and P. Taels, *Photoproduction of three jets in the CGC: gluon TMDs and dilute limit*, *JHEP* **07** (2020) 143, [[2001.00765](#)].
- [141] J. C. Collins and R. Ellis, *Heavy quark production in very high-energy hadron collisions*, *Nucl. Phys. B* **360** (1991) 3–30.
- [142] S. Catani, M. Ciafaloni and F. Hautmann, *High-energy factorization and small x heavy flavor production*, *Nucl. Phys. B* **366** (1991) 135–188.
- [143] M. Ciafaloni, *Coherence Effects in Initial Jets at Small q^{*2} / s* , *Nucl. Phys. B* **296** (1988) 49–74.
- [144] S. Catani, F. Fiorani and G. Marchesini, *Small x Behavior of Initial State Radiation in Perturbative QCD*, *Nucl. Phys. B* **336** (1990) 18–85.
- [145] A. van Hameren, P. Kotko and K. Kutak, *Helicity amplitudes for high-energy scattering*, *JHEP* **01** (2013) 078, [[1211.0961](#)].
- [146] CASCADE collaboration, S. Baranov et al., *CASCADE3 A Monte Carlo event generator based on TMDs*, *Eur. Phys. J. C* **81** (2021) 425, [[2101.10221](#)].
- [147] A. van Hameren, P. Kotko and K. Kutak, *Multi-gluon helicity amplitudes with one off-shell leg within high energy factorization*, *JHEP* **12** (2012) 029, [[1207.3332](#)].
- [148] P. Kotko, *Wilson lines and gauge invariant off-shell amplitudes*, *JHEP* **07** (2014) 128, [[1403.4824](#)].
- [149] A. van Hameren, *BCFW recursion for off-shell gluons*, *JHEP* **07** (2014) 138, [[1404.7818](#)].
- [150] A. van Hameren and M. Serino, *BCFW recursion for TMD parton scattering*, *JHEP* **07** (2015) 010, [[1504.00315](#)].
- [151] M. Deak, F. Hautmann, H. Jung and K. Kutak, *Forward Jet Production at the Large Hadron Collider*, *JHEP* **09** (2009) 121, [[0908.0538](#)].

- [152] R. Angeles-Martinez et al., *Transverse Momentum Dependent (TMD) parton distribution functions: status and prospects*, *Acta Phys. Polon. B* **46** (2015) 2501–2534, [[1507.05267](#)].
- [153] R. Boussarie et al., *TMD Handbook*, [2304.03302](#).
- [154] C. J. Bomhof, P. J. Mulders and F. Pijlman, *The Construction of gauge-links in arbitrary hard processes*, *Eur. Phys. J. C* **47** (2006) 147–162, [[hep-ph/0601171](#)].
- [155] M. Bury, P. Kotko and K. Kutak, *TMD gluon distributions for multiparton processes*, *Eur. Phys. J. C* **79** (2019) 152, [[1809.08968](#)].
- [156] B.-W. Xiao and F. Yuan, *Non-Universality of Transverse Momentum Dependent Parton Distributions at Small- x* , *Phys. Rev. Lett.* **105** (2010) 062001, [[1003.0482](#)].
- [157] F. Dominguez, C. Marquet, B.-W. Xiao and F. Yuan, *Universality of Unintegrated Gluon Distributions at small x* , *Phys. Rev. D* **83** (2011) 105005, [[1101.0715](#)].
- [158] A. Metz and J. Zhou, *Distribution of linearly polarized gluons inside a large nucleus*, *Phys. Rev. D* **84** (2011) 051503, [[1105.1991](#)].
- [159] E. Akcakaya, A. Schäfer and J. Zhou, *Azimuthal asymmetries for quark pair production in pA collisions*, *Phys. Rev. D* **87** (2013) 054010, [[1208.4965](#)].
- [160] I. Balitsky and A. Tarasov, *Rapidity evolution of gluon TMD from low to moderate x* , *JHEP* **10** (2015) 017, [[1505.02151](#)].
- [161] I. Balitsky and A. Tarasov, *Gluon TMD in particle production from low to moderate x* , *JHEP* **06** (2016) 164, [[1603.06548](#)].
- [162] Y. V. Kovchegov and M. D. Sievert, *Calculating TMDs of a Large Nucleus: Quasi-Classical Approximation and Quantum Evolution*, *Nucl. Phys. B* **903** (2016) 164–203, [[1505.01176](#)].
- [163] Y. V. Kovchegov, D. Pitonyak and M. D. Sievert, *Helicity Evolution at Small- x* , *JHEP* **01** (2016) 072, [[1511.06737](#)].
- [164] Y. V. Kovchegov, D. Pitonyak and M. D. Sievert, *Small- x Asymptotics of the Gluon Helicity Distribution*, *JHEP* **10** (2017) 198, [[1706.04236](#)].
- [165] Y. V. Kovchegov and M. D. Sievert, *Small- x Helicity Evolution: an Operator Treatment*, *Phys. Rev. D* **99** (2019) 054032, [[1808.09010](#)].
- [166] R. Boussarie and Y. Mehtar-Tani, *A novel formulation of the unintegrated gluon distribution for DIS*, *Phys. Lett. B* **831** (2022) 137125, [[2006.14569](#)].
- [167] R. Boussarie and Y. Mehtar-Tani, *Gluon-mediated inclusive Deep Inelastic Scattering from Regge to Bjorken kinematics*, *JHEP* **07** (2022) 080, [[2112.01412](#)].
- [168] C. Marquet, E. Petreska and C. Roiesnel, *Transverse-momentum-dependent gluon distributions from JIMWLK evolution*, *JHEP* **10** (2016) 065, [[1608.02577](#)].
- [169] T. Altinoluk and R. Boussarie, *Low x physics as an infinite twist (G)TMD framework: unravelling the origins of saturation*, *JHEP* **10** (2019) 208, [[1902.07930](#)].
- [170] T. Altinoluk, R. Boussarie and P. Kotko, *Interplay of the CGC and TMD frameworks to all orders in kinematic twist*, *JHEP* **05** (2019) 156, [[1901.01175](#)].
- [171] M. L. Mangano and S. J. Parke, *Multiparton amplitudes in gauge theories*, *Phys. Rept.* **200** (1991) 301–367, [[hep-th/0509223](#)].
- [172] T. Altinoluk, C. Marquet and P. Taels, *Low- x improved TMD approach to the lepto- and hadroproduction of a heavy-quark pair*, *JHEP* **06** (2021) 085, [[2103.14495](#)].

- [173] R. Boussarie, H. Mäntysaari, F. Salazar and B. Schenke, *The importance of kinematic twists and genuine saturation effects in dijet production at the Electron-Ion Collider*, *JHEP* **09** (2021) 178, [[2106.11301](#)].
- [174] M. Bury, A. van Hameren, P. Kotko and K. Kutak, *Forward trijet production in p - p and p - Pb collisions at LHC*, *JHEP* **09** (2020) 175, [[2006.13175](#)].
- [175] A. van Hameren, *KaTie : For parton-level event generation with k_T -dependent initial states*, *Comput. Phys. Commun.* **224** (2018) 371–380, [[1611.00680](#)].
- [176] J. Alwall et al., *A Standard format for Les Houches event files*, *Comput. Phys. Commun.* **176** (2007) 300–304, [[hep-ph/0609017](#)].
- [177] N. A. Abdulov et al., *TMDlib2 and TMDplotter: a platform for 3D hadron structure studies*, *Eur. Phys. J. C* **81** (2021) 752, [[2103.09741](#)].
- [178] F. Caravaglios and M. Moretti, *An algorithm to compute Born scattering amplitudes without Feynman graphs*, *Phys. Lett. B* **358** (1995) 332–338, [[hep-ph/9507237](#)].
- [179] M. L. Mangano, M. Moretti, F. Piccinini, R. Pittau and A. D. Polosa, *ALPGEN, a generator for hard multiparton processes in hadronic collisions*, *JHEP* **07** (2003) 001, [[hep-ph/0206293](#)].
- [180] M. A. Kimber, J. Kwiecinski and A. D. Martin, *Gluon shadowing in the low x region probed by the LHC*, *Phys. Lett. B* **508** (2001) 58–64, [[hep-ph/0101099](#)].
- [181] K. Kutak and J. Kwiecinski, *Screening effects in the ultrahigh-energy neutrino interactions*, *Eur. Phys. J. C* **29** (2003) 521, [[hep-ph/0303209](#)].
- [182] N. N. Nikolaev and W. Schafer, *Quenching of Leading Jets and Particles: The p perp Dependent Landau-Pomeranchuk-Migdal effect from Nonlinear k perp Factorization*, *Phys. Rev. D* **74** (2006) 014023, [[hep-ph/0604117](#)].
- [183] J. Kwiecinski, A. D. Martin and A. Stasto, *A Unified BFKL and GLAP description of F_2 data*, *Phys. Rev. D* **56** (1997) 3991–4006, [[hep-ph/9703445](#)].
- [184] H1, ZEUS collaboration, F. Aaron et al., *Combined Measurement and QCD Analysis of the Inclusive e^+p Scattering Cross Sections at HERA*, *JHEP* **01** (2010) 109, [[0911.0884](#)].
- [185] S. Bondarenko, *Gluon density and $F(2)$ functions from BK equation with impact parameter dependence*, *Phys. Lett. B* **665** (2008) 72–78, [[0802.1802](#)].
- [186] A. Mueller, B.-W. Xiao and F. Yuan, *Sudakov double logarithms resummation in hard processes in the small- x saturation formalism*, *Phys. Rev. D* **88** (2013) 114010, [[1308.2993](#)].
- [187] A. H. Mueller, L. Szymanowski, S. Wallon, B.-W. Xiao and F. Yuan, *Sudakov Resummations in Mueller-Navelet Dijet Production*, *JHEP* **03** (2016) 096, [[1512.07127](#)].
- [188] A. Mueller, B. Wu, B.-W. Xiao and F. Yuan, *Medium Induced Transverse Momentum Broadening in Hard Processes*, *Phys. Rev. D* **95** (2017) 034007, [[1608.07339](#)].
- [189] A. Mueller, B.-W. Xiao and F. Yuan, *Sudakov Resummation in Small- x Saturation Formalism*, *Phys. Rev. Lett.* **110** (2013) 082301, [[1210.5792](#)].
- [190] C. Marquet, S.-Y. Wei and B.-W. Xiao, *Probing parton saturation with forward Z^0 -boson production at small transverse momentum in $p+p$ and $p+A$ collisions*, *Phys. Lett. B* **802** (2020) 135253, [[1909.08572](#)].
- [191] A. van Hameren, P. Kotko, K. Kutak and S. Sapeta, *Small- x dynamics in forward-central dijet decorrelations at the LHC*, *Phys. Lett. B* **737** (2014) 335–340, [[1404.6204](#)].
- [192] P. Sun, J. Isaacson, C. P. Yuan and F. Yuan, *Nonperturbative functions for SIDIS and Drell–Yan processes*, *Int. J. Mod. Phys. A* **33** (2018) 1841006, [[1406.3073](#)].

- [193] G. Watt, A. Martin and M. Ryskin, *Unintegrated parton distributions and inclusive jet production at HERA*, *Eur. Phys. J. C* **31** (2003) 73–89, [[hep-ph/0306169](#)].
- [194] A. van Hameren, P. Kotko, K. Kutak, C. Marquet, E. Petreska and S. Sapeta, *Forward di-jet production in p+Pb collisions in the small-x improved TMD factorization framework*, *JHEP* **12** (2016) 034, [[1607.03121](#)].
- [195] M. A. Al-Mashad, A. van Hameren, H. Kakkad, P. Kotko, K. Kutak, P. van Mechelen et al., *Dijet azimuthal correlations in p-p and p-Pb collisions at forward LHC calorimeters*, *JHEP* **12** (2022) 131, [[2210.06613](#)].
- [196] H. Fujii, C. Marquet and K. Watanabe, *Comparison of improved TMD and CGC frameworks in forward quark dijet production*, *JHEP* **12** (2020) 181, [[2006.16279](#)].
- [197] M. A. Al-Mashad, A. van Hameren, H. Kakkad, P. Kotko, K. Kutak, P. van Mechelen et al., *Dijet azimuthal correlations in p-p and p-pb collisions at forward lhc calorimeters*, 2022.
- [198] M. Cacciari, G. P. Salam and G. Soyez, *The anti- k_t jet clustering algorithm*, *JHEP* (04, 2008) , [[0802.1189](#)].
- [199] H.-L. Lai, M. Guzzi, J. Huston, Z. Li, P. M. Nadolsky, J. Pumplin et al., *New parton distributions for collider physics*, *Physical Review D* **82** (oct, 2010) .
- [200] A. Buckley, J. Ferrando, S. Lloyd, K. Nordström, B. Page, M. Rüfenacht et al., *LHAPDF6: parton density access in the LHC precision era*, *The European Physical Journal C* **75** (mar, 2015) .
- [201] T. Sjöstrand, S. Mrenna and P. Z. Skands, *PYTHIA 6.4 Physics and Manual*, *JHEP* **05** (2006) 026, [[0603175](#)].
- [202] T. Sjöstrand, S. Ask, J. R. Christiansen et al., *An Introduction to PYTHIA 8.2*, *Comput. Phys. Commun.* **191** (2015) 159–177, [[1410.3012](#)].
- [203] M. Bury, A. van Hameren, H. Jung, K. Kutak, S. Sapeta and M. Serino, *Calculations with off-shell matrix elements, TMD parton densities and TMD parton showers*, *Eur. Phys. J. C* **78** (2018) 137, [[1712.05932](#)].
- [204] M. Arratia, Y. Song, F. Ringer and B. V. Jacak, *Jets as precision probes in electron-nucleus collisions at the future Electron-Ion Collider*, *Phys. Rev. C* **101** (2020) 065204, [[1912.05931](#)].
- [205] H. T. Li and I. Vitev, *Nuclear matter effects on jet production at electron-ion colliders*, [2010.05912](#).
- [206] F. Bergabo and J. Jalilian-Marian, *Single inclusive hadron production in DIS at small x: next to leading order corrections*, *JHEP* **01** (2023) 095, [[2210.03208](#)].
- [207] F. Bergabo and J. Jalilian-Marian, *Dihadron production in DIS at small x at next-to-leading order: Transverse photons*, *Phys. Rev. D* **107** (2023) 054036, [[2301.03117](#)].
- [208] P. Kotko, K. Kutak, S. Sapeta, A. M. Stasto and M. Strikman, *Estimating nonlinear effects in forward dijet production in ultra-peripheral heavy ion collisions at the LHC*, *Eur. Phys. J. C* **77** (2017) 353, [[1702.03063](#)].
- [209] A. van Hameren, P. Kotko, K. Kutak, S. Sapeta and E. Żarów, *Probing gluon number density with electron-dijet correlations at EIC*, *Eur. Phys. J. C* **81** (2021) 741, [[2106.13964](#)].
- [210] T. Goda, K. Kutak and S. Sapeta, *Effects of gluon kinematics and the Sudakov form factor on the dipole amplitude*, [2305.14025](#).
- [211] M. Hentschinski et al., *White Paper on Forward Physics, BFKL, Saturation Physics and Diffraction*, *Acta Phys. Polon. B* **54** (2023) 2, [[2203.08129](#)].

- [212] J. L. Albacete, G. Giacalone, C. Marquet and M. Matas, *Forward dihadron back-to-back correlations in pA collisions*, *Phys. Rev. D* **99** (2019) 014002, [[1805.05711](#)].
- [213] J. Jalilian-Marian and A. H. Rezaeian, *Hadron production in pA collisions at the LHC from the Color Glass Condensate*, *Phys. Rev. D* **85** (2012) 014017, [[1110.2810](#)].
- [214] B. Ducloué, T. Lappi and H. Mäntysaari, *Forward J/ψ production in proton-nucleus collisions at high energy*, *Phys. Rev. D* **91** (2015) 114005, [[1503.02789](#)].
- [215] M. Hentschinski, J. D. Madrigal Martínez, B. Murdaca and A. Sabio Vera, *NLO Vertex for a Forward Jet plus a Rapidity Gap at High Energies*, *AIP Conf. Proc.* **1654** (2015) 070013, [[1409.7731](#)].
- [216] E. Blanco, A. van Hameren, P. Kotko and K. Kutak, *All-plus helicity off-shell gauge invariant multigluon amplitudes at one loop*, *JHEP* **12** (2020) 158, [[2008.07916](#)].
- [217] A. van Hameren, L. Motyka and G. Ziarko, *Hybrid k_T -factorization and impact factors at NLO*, *JHEP* **11** (2022) 103, [[2205.09585](#)].
- [218] E. Blanco, A. Giachino, A. van Hameren and P. Kotko, *One-loop gauge invariant amplitudes with a space-like gluon*, [2212.03572](#).
- [219] M. Hentschinski, A. Sabio Vera and C. Salas, *Hard to Soft Pomeron Transition in Small- x Deep Inelastic Scattering Data Using Optimal Renormalization*, *Phys. Rev. Lett.* **110** (2013) 041601, [[1209.1353](#)].
- [220] E. Iancu, J. D. Madrigal, A. H. Mueller, G. Soyez and D. N. Triantafyllopoulos, *Collinearly-improved BK evolution meets the HERA data*, *Phys. Lett. B* **750** (2015) 643–652, [[1507.03651](#)].
- [221] M. Hentschinski, A. Kusina and K. Kutak, *Transverse momentum dependent splitting functions at work: quark-to-gluon splitting*, *Phys. Rev. D* **94** (2016) 114013, [[1607.01507](#)].
- [222] M. Hentschinski, A. Kusina, K. Kutak and M. Serino, *TMD splitting functions in k_T factorization: the real contribution to the gluon-to-gluon splitting*, *Eur. Phys. J. C* **78** (2018) 174, [[1711.04587](#)].
- [223] Y. Shi, L. Wang, S.-Y. Wei and B.-W. Xiao, *Pursuing the Precision Study for Color Glass Condensate in Forward Hadron Productions*, *Phys. Rev. Lett.* **128** (2022) 202302, [[2112.06975](#)].
- [224] W. Li and A. M. Stasto, *Structure functions from renormalization group improved small x evolution*, *Eur. Phys. J. C* **82** (2022) 562, [[2201.10579](#)].
- [225] F. Hautmann, M. Hentschinski, L. Keersmaekers, A. Kusina, K. Kutak and A. Lelek, *A parton branching with transverse momentum dependent splitting functions*, *Phys. Lett. B* **833** (2022) 137276, [[2205.15873](#)].
- [226] C. Marquet, C. Roiesnel and P. Taels, *Linearly polarized small- x gluons in forward heavy-quark pair production*, *Phys. Rev. D* **97** (2018) 014004, [[1710.05698](#)].